CODEN:LUTEDX/(TEIE-7269)/1-50/(2017)

Industrial Electrical Engineering and Automation

Plant-wide model-based analysis of simultaneous precipitation on phosphorus removal in an activated sludge system with MBRs

Christian Kazadi Mbamba and Ulf Jeppsson

Division of Industrial Electrical Engineering and Automation
Faculty of Engineering, Lund University

TECHNICAL REPORT

Plant-wide model-based analysis of simultaneous precipitation on phosphorus removal in an activated sludge system with MBRs

Dr Christian Kazadi Mbamba, Assoc. Prof Ulf Jeppsson

LUND UNIVERSITY

December 2017

Approved by: Stockholm Water and Waste AB

TABLE OF CONTENTS

Executive summary

Wastewater treatment technologies combined with membrane bioreactors and chemical precipitation are gaining wide acceptance as a suitable pathway when very low effluent phosphorus concentrations are the treatment target. A modelling study was carried out to evaluate operational and control strategies for such a pilot scale system. The main purpose of this work was to describe the use of iron salts (ferrous or ferric iron) in membrane bioreactors (MBRs) and focuses on questions of possible interference with the biological mechanisms arising from the addition of these iron precipitants. The specific objectives of the study are to: (1) predict accurately the dynamic behaviour of the pilot plant (with MBR and chemical precipitation); (2) perform dynamic simulations with the calibrated plant-wide model to further increase understanding of underlying principles of the integrated system and provide information for optimizing design and operations applicable to full-scale systems.

Sub-models from a recently upgraded version of the Benchmark Simulation Model No. 2 with an improved/expanded physico-chemical framework were used to develop the plant-wide model for the pilot plant. The physico-chemical module includes an equilibrium approach describing ion speciation and ion pairing, kinetic minerals precipitation (such as hydrous ferric oxides (HFO) and $FePO_4$) as well as adsorption and co-precipitation. Model performance was evaluated against data sets from a pilot plant, assessing the capability to describe water and sludge lines across the treatment process under steady-state operation.

With default rate kinetic and stoichiometric parameters, a good general agreement was observed between the pilot-scale datasets and the simulated results under steady-state conditions. Simulation results showed differences between measured and modelled phosphorus as little as 5–10% (relative) throughout the entire plant. The study also showed that environmental factors, such as pH as well as Fe/P molar ratios (1, 1.5 and 2), influence the concentration of dissolved phosphate in the effluent. The time constant of simultaneous precipitation, in the calibrated model, due to $FeSO_4$ step change (decrease/increase) was found to be roughly 5 days, indicating a slow dynamic response due to multi-steps involving dissolution, oxidation, precipitation, aging, adsorption and co-precipitation processes. The persistence effect of accumulated iron-precipitates (HFO particulates) in the activated sludge was likely responsible for phosphorus removal and therefore the solid retention time plays a crucial role. In order words, the reactivity of these iron-precipitates cycling in the MBR

system over an extended period was apparently maintained through alternation of the sludge between anoxic and aerobic conditions.

Dynamic influent profiles were generated using a calibrated influent generator and were used to study the effect of long-term influent dynamics on plant performance. Model-based analyses showed that controlling the addition of coagulants strongly influenced the phosphorus removal in the activated sludge system, while the aerobic tank deemed to be the most suitable dosing location for $FeSO_4$ addition due to high oxidizing and good mixing conditions.

The dynamic plant-wide model is a promising engineering tool that can be used to optimize system design and operational aspects, such as control of chemical dosage under dynamic loading conditions. This aspect is important as far as maintaining suitable biological nutrient removal in the activated sludge systems.

Nomenclature

Ac^-	Acetate ion	($g.m^{-3}$)
ADM1	Anaerobic Digestion Model No. 1	
a_i	Chemical activities	
Al^{+3}	Aluminium ion	
ASM	Activated sludge model	
ASM2d	Activated sludge model No 2	
BAP	Biomass associated products	
BOD_7	7-day Biochemical Oxygen Demand	($gCOD.m^{-3}$)
BR1/ANOX	Anoxic bioreactor 1	
BR2/ANOX	Anoxic bioreactor 2	
BR3/FLEX	Swing bioreactor 3 (anoxic/aerobic)	
BR4/AERO	Aerobic bioreactor 4	
BR5/AERO	Aerobic bioreactor 5	
BR6/DEOX	De-aeration bioreactor 6	
BR7/ANOX	Post-anoxic bioreactor 7	
BSM2	Benchmark Simulation Model No. 2	
Bu^-	Buturate ion	($moles.L^{-1}$)
Ca^{2+}	Calcium ion	($moles.L^{-1}$)
CAS	Conventional activated sludge	
Cl^-	Chloride ion	($moles.L^{-1}$)
CO_2	Carbon dioxide	
CO_3^{-2}	Carbonate	($moles.L^{-1}$)
COD	Chemical oxygen demand	($gCOD.m^{-3}$)
DO	Dissolved oxygen	($g.m^{-3}$)
EBPR	Enhanced biological phosphorus process removal	
EPA	Environmental Protection Agency	
Fe	Iron	
$FeCl_3$	Iron chloride	
$FeSO_4$	Iron(II) sulphate	
HS^-	Sulphide	($moles.L^{-1}$)
Iron(II) or	Ferrous iron	($moles.L^{-1}$)

Fe^{2+}		
Iron(III) or Fe^{3+}	Ferric iron	(moles.L^{-1})
ISS	Inorganic suspended solids	(gSS.m^{-3})
K^+	Potassium ion	(moles.L^{-1})
k_{cryst}	Precipitation kinetic rate parameter	(d^{-1})
k_{FePO4}	Rate of iron phosphate precipitation	(d^{-1})
K_i	Equilibrium constant	
K_{sp}	Solubility product constant	
$K_{spFePO4}$	Solubility constant for iron phosphate	
MBR	Membrane bioreactor	
Mg	Magnesium	
Mg^{2+}	Magnesium ion	(mole.L^{-1})
MLSS	Mixed liquor suspended solids	(mole.L^{-1})
n	Order of the precipitation reaction	
Na	Sodium	
Na^+	Sodium ion	(mole.L^{-1})
NH_3	Ammonia	
NH_4^+	Ammonium ion	(mole.L^{-1})
NH_4-*N*	Ammonia nitrogen	(gN.m^{-3})
NO_2^-	Nitrite	
NO_3-*N*	Nitrate nitrogen	(gN.m^{-3})
O_2	Oxygen	
pH	Hydrogen potential	(Standard)
PO_4^{-3}	Phosphate	
PO4-P	Orthophosphorus	(gP.m^{-3})
Pro^-	Propionate	(gP.m^{-3})
RAS	Returned activated sludge	
r_{FePO4}	Rate of iron phosphate precipitation	(d^{-1})
S_A	Fermentation products	(gCOD.m^{-3})
S_F	Readily biodegradable	(gCOD.m^{-3})
S_I	Inert biodegradable organics	(gCOD.m^{-3})
SMP	Soluble microbial product	(g.m^{-3})

S_{O2}	Dissolved oxygen,	($g.m^{-3}$)
SO_4^{-2}	Sulphate	($g.m^{-3}$)
T	Time	(min, h, day)
T	Temperature	(^oC, K)
TIC	Total inorganic carbon	($gC.m^{-3}$)
TN	Total nitrogen	($gN.m^{-3}$)
TOC	Total organic carbon	($gC.m^{-3}$)
TOT_j	Species contribution balance	($moles.L^{-1}$)
TP	Total phosphorus	($gP.m^{-3}$)
TSS	Total suspended solid	($gSS.m^{-3}$)
UAP	Utilization-associated products	($gCOD.m^{-3}$)
Va^-	Valerate	($gCOD.m^{-3}$)
VFA	Volatile fatty acids	($gCOD.m^{-3}$)
VSS	Volatile suspended solids	($gSS.m^{-3}$)
WAS	Waste activated sludge	
$WWTP$	Wastewater treatment pant	
X_{AUT}	Autotrophic biomass	($gCOD.m^{-3}$)
X_{FePO4}	Iron phosphate mineral state	($gFe.m^{-3}$)
X_H	Heterotrophic biomass	($gCOD.m^{-3}$)
X_{HFO}	Hydrous ferric oxide	($g.m^{-3}$)
$X_{HFO,H}$	Hydrous ferric oxide with high adsorption capacity	($g.m^{-3}$)
$X_{HFO,H,P}$	$X_{HFO,H}$ with adsorbed phosphate	($g.m^{-3}$)
$X_{HFO,L}$	Hydrous ferric oxide with low adsorption capacity	($g.m^{-3}$)
$X_{HFO,L,P}$	$X_{HFO,L}$ with adsorbed phosphate	($g.m^{-3}$)
X_I	Inert non-biodegradable organics	($gCOD.m^{-3}$)
X_{ISS}	Inorganic suspended solid state	($gSS.m^{-3}$)
X_{PAO}	Phosphorus-accumulating organism state	($gCOD.m^{-3}$)
X_{PHA}	Polyhydroxy-alkanoate state	($gCOD.m^{-3}$)
X_{PP}	Polyphosphate state	($g.m^{-3}$)
X_S	Slowly biodegradable substrate state	($gCOD.m^{-3}$)
X_{TSS}	Total suspended solid state	($gTSS.m^{-3}$)

y	Experimentally measured output	
$Z_{(Fe3+)}$	Chemical activity of ferric iron	
$Z_{(PO43-),}$	Chemical activity of phosphate	
z_i	Charge valency of ionic species i	
Z_i	Concentration of ionic species i	(mole.L^{-1})
Z_j	Concentration of iterative species	(mole.L^{-1})
γ	Activity coefficient	
σ	Supersaturation	

1. Background and scope of work

In recent years, effluent discharge guidelines to receiving waters are becoming more stringent owing to increased awareness and growing concerns regarding pollution and degradation of waters and freshwaters. Current effluent standards in Stockholm, Sweden, restrict the concentrations of P in treated wastewater discharge to less than 0.3 $gP.m^{-3}$. However, these requirements are expected to be sharpened for more efficient phosphorus removal. The future emission standards for total phosphorus in Stockholm, Sweden, will be around 0.2 $gP.m^{-3}$ while the annual average effluent target would be set at 0.15 $gP.m^{-3}$ (Anderson *et al*., 2016). To meet stricter quality standards, the effluent should contain very low concentrations of dissolved phosphorus and almost no suspended solids. Such aspects will lead wastewater treatment facilities to undergo significant modifications and improvements as far as nutrient removal is concerned. A number of existing wastewater treatment plants are now attracted to nutrient removal using conventional activated sludge (CAS) systems coupled with membrane bioreactors (MBRs) (Judd, 2008). Since MBR systems have high selectivity, high suspended solids concentrations and high sludge retention times as well as smaller footprint, biological nutrient removal in MBRs is therefore becoming more popular as a means of treating wastewater and has been successfully achieved at lab-, pilot- and full-scale (Daigger *et al.*, 2010; Wang *et al.*, 2014).

Achieving very low P effluent concentrations through biological processes, such as enhanced biological process removal (EBPR), depends on a number of factors including having favourable wastewater characteristics and optimal environmental conditions. However, the feasibility of EBPR systems may be limited to some extent (Ekama, 2010). In such situations, P removal by biological means can be complemented or fully replaced by chemical precipitation processes (De Haas *et al.*, 2000a). In current practice, chemical phosphorus removal in activated sludge plants is mainly performed by the addition of iron or aluminum salts at the pre-aeration step (pre-precipitation) to raw sewage, in the activated sludge tanks (simultaneous precipitation or co-precipitation) to mixed liquor or/and at the tertiary processes (post-precipitation) (Henze *et al.*, 2002; EPA, 2010). The phosphorus removal efficiency depends on a number of factors including pH, temperature, dosing location, reactor configuration and microorganisms present in a specific wastewater (De Haas *et al.*, 2000a; Wang *et al.*, 2014). In return, these factors will dictate the forms of iron (either Fe^{3+} or Fe^{2+}) and influence the rate and extent of their transformations. As an illustration, when Fe(III) salts are added to the mixed liquor, they will ionize to yield the free metallic ions, a portion of

which may react with orthophosphate (PO_4-P) to form insoluble Fe(III) precipitates (strengite), which are then separated by sedimentation (Wu *et al.*, 2015). However, the majority of ferric ions will combine with hydroxide ions to form a variety of hydroxide complexes, termed hydrous ferric oxides (HFO) with high sorption, which will subsequently assist in the removal of phosphorus by adsorption and co-precipitation (Hauduc *et al.*, 2015). Due to high costs of ferric iron, Fe salts are in some instance added as Fe(II), such as $FeSO_4$, which may oxidize to Fe^{3+} (Fe(III)) at the dosing point if oxidizing conditions prevail in the biological treatment stage (EPA, 2010). In order to achieve greater degrees of P removal stipulated in an environmental discharge licence in the future, higher levels of iron dosing may be required. In comparison to current discharge requirements, this means the activated sludge treatment plants will have to operate with much lower phosphorus concentrations, which may inhibit biological activities, such as nitrification and denitrification processes due to shortage of phosphorus, an essential nutrient for microbial growth (Philips *et al.*, 2003). Thus, finding optimal control and operational conditions is key to efficient phosphorus removal from wastewater.

An insight into the interactions between iron species and phosphorus within a biological nutrient system with membrane separation is of particular importance to Sweden. Stockholm's Water and Waste company (SVOA) is currently assessing at pilot-scale biological nutrient removal with MBRs. The purpose of conducting pilot-plant studies is to establish a suitable treatment pathway in line with stricter discharge requirements in the future. This goal should be achieved without any major volumetric upgrade of the current full-scale treatment plant, which is mainly underground in constructed rock caverns (Anderson *et al.*, 2016). The pilot-tests have significantly increased knowledge of the process design with membrane technology and modified biological treatment that will be introduced at Henriksdal WWTP as part of SVOA's future sewage treatment. However, there is still a need to further clarify the impacts of ferric and ferrous iron dosing on phosphorus removal in the activated sludge system. Understanding iron speciation and transformation through modelling is critical to capture the mechanism of iron-precipitates, as their nature, movement and fate in the bioreactors would influence both phosphorus removal efficiency as well as membrane performance characteristics. In the present study, current modelling approaches and understanding of the reaction mechanisms of iron and P are applied to pilot-scale data to evaluate control and operational strategies. The study also focuses on the impact of Fe/P molar ratio system when the pH varies and their effects on effluent concentration of total P,

for example due to routine membrane cleaning with acidic solutions. Furthermore, this work intends to determine and explain (theoretically) the differing performance of precipitation with respect to dosing Fe^{3+} compared with dosing Fe^{2+}, the different effects on the residual total phosphorus in the effluent as well as to determine the time constants of the system and how these are related to the residence time and sludge age.

The present report focuses on pilot-plant modelling and is one of the deliverables of this project. Two other deliverables include two plant-wide modelling tools for the pilot-plant and the existing full-scale Henriksdal WWTP. The report is structured to first present the underlying principles of the plant-wide model including the precipitation model, then the validation step with static pilot-test data and other steady-state analyses, after which dynamic simulations are used to examine the influence of operational and control factors.

2 Methodology

2.1 Pilot plant under study

The modelled MBR pilot-plant is located at the R&D facility Hammarby Sjöstadsverk, which is adjacent to the Henriksdal wastewater treatment plant at Henriksdalsberget, Stockholm (Sweden). The purpose of the pilot plant was to evaluate the design and optimize the operation and control. Its design mimics the configuration of the future full-scale facility, which consists of pre-aeration, pre-sedimentation, anoxic, aeration zones and membrane bioreactors. The scale factor used in the design and rebuilding of the pilot plant compared with the full-scale plant is 1:6,700, except for the primary sedimentation, which is relatively small (scale factor 1:12,000), and as a result led to poorer TSS separation efficiency. A major difference for operating strategy and control is that the pilot has only two membrane tanks that can be put into operation for optimal / energy efficient membrane operation, whereas each line in the full-scale system will have 12 membrane tanks.

Figure 1 presents a simplified schematic flow diagram of the pilot-plant treatment process. It consists of a conventional primary treatment including a pre-aeration step, where $FeSO_4$ is added, followed by seven bioreactors operated as a 4-stage modified Ludzack-Ettinger (MLE) process consisting of two anoxic (BR1/ANOX and BR2/ANOX), one aerobic/anoxic (BR3/FLEX), two aerobic (BR4/AERO and BR5/AERO), one de-aeration (BR6/DEOX) and one post-anoxic (BR7/ANOX) compartment. The dimensions of each reactor are presented in Table 1. The Henriksdal wastewater treatment plant consists of two influents: Sickla influent (SIN) and Henriksdal influent (HIN). The influent to the pilot-plant was derived from HIN.

The mixed liquor suspended solids (MLSS) are treated in the membrane bioreactor tanks to produce clarified permeate for final discharge. On the other hand, the retentate from the MBRs are distributed to the bioreactors as returned activated sludge (RAS) as well as waste activated sludge (WAS), which is pumped at a flow rate of 1.3 m^3 d^{-1}. A sludge treatment facility was underway at the pilot plant but not in operation during this project; however, anaerobically digested supernatant (Table 2) from Henriksdal WWTP was blended with the RAS flow in the RAS-deox zone and then fed to the first anoxic reactor.

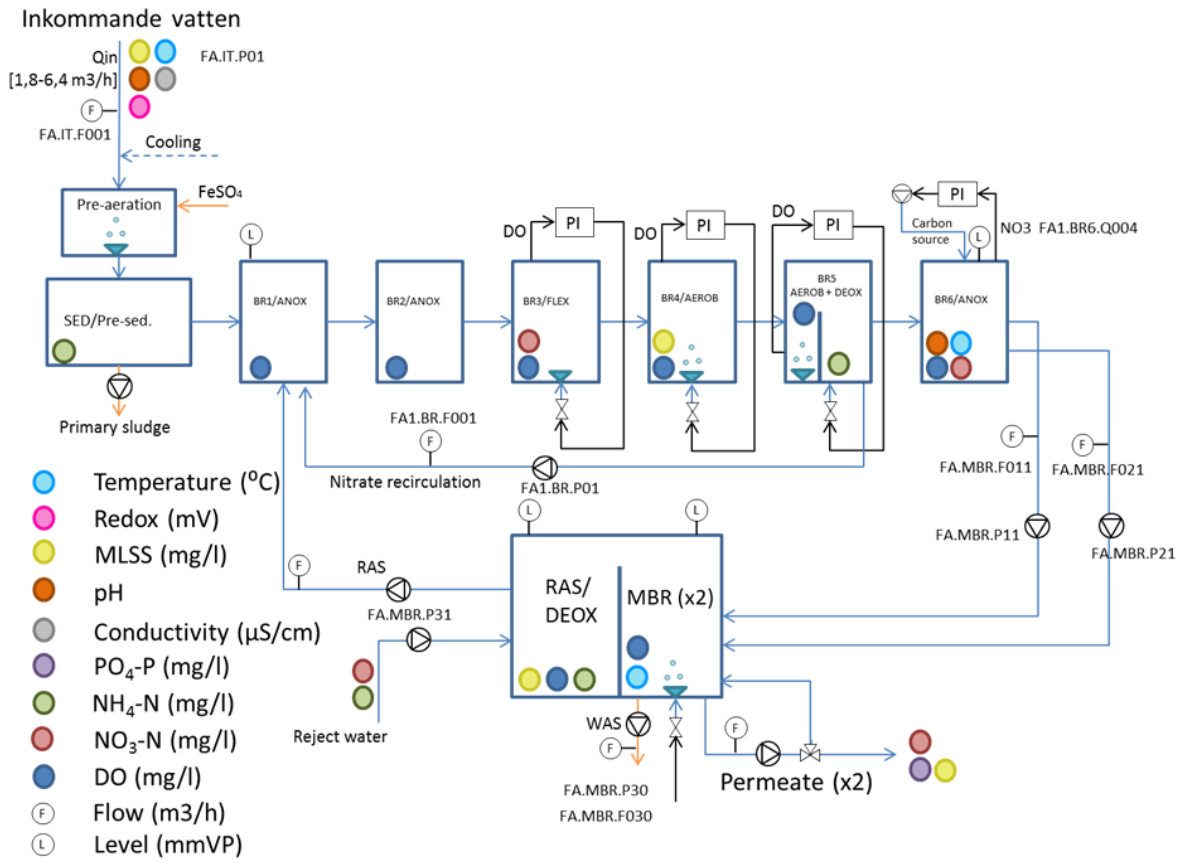

Figure 1 *– Schematic process diagram of the pilot-plant treatment process.*

Table 1 *– Configuration of the physical compartments in the activated sludge plant.*

Activated sludge zone	**Physical tank volume (m^3)**
Anoxic (BR1/ANOx)	4.8
Anoxic (BR2/ANOx)	4.8
Anoxic/Aerobic Swing (BR3/FLEX)	4.8
Aerobic (BR4/AEROB)	4.8
Aerobic (BR5/AEROB)	1.5
De-aeration (BR5/DEOX)	3.3
Post-anoxic (BR6/ANOX)	4.8
MBR1	1.45
MBR2	1.45
RAS deoxygenation (RAS/DEOX)	2.7

Table 2 *– Composition of the supernatant from the full-scale anaerobic digesters at Henriksdal WWTP.*

Parameters	**Values**
Total COD (gCOD.m^{-3})	502
Soluble COD (gCOD.m^{-3})	337
Total nitrogen (gN.m^{-3})	523
Ammonia nitrogen (gN.m^{-3})	460
Total phosphorus (gP.m^{-3})	18.2
Orthophosphorus (gP.m^{-3})	1.60
Total iron (gFe.m^{-3})	1.10
Total suspended solids (gSS.m^{-3})	1560

2.2 Membrane bioreactors

The MBR pilot use hollow fiber membranes from GE with nominal pore size 0.04 μm. The diaphragm pilot consists of two cassettes (2.5m x 1.0m x 0.34m) consisting of three membrane modules each, immersed in each tank. Each module has a membrane area of 34.2 m^2 and consists of a variety of fiber strands with attachment at the top and bottom of the cassette frame. The filtered water (permeate) is transported on the inside of the fibers to connections in both the bottom and the top of the module. The membranes were kept clean during operation by aeration from below. The bioreactors were operated with a HRT of 12 h and a SRT of about 23 days. The membrane modules were operated in intermittent mode with 9 min of filtration followed by 1 min relaxation at a constant flux of 19.4 L.m^{-2}.h^{-1} (LMH). A summary of the design and operating conditions is presented in Table 3.

Table 3 *– Design and operating parameters of the membrane bioreactors.*

Parameters	**Pilot scale MBR**
Volume per MBR (m^3)	1.45
Membrane nominal pore size (μm)	0.04
Membrane area per module (m^2)	34.4
Average filtration flux (L.m^{-2}.h^{-1})	19.4
Hydraulic retention time (h)	12
Solid retention time (d)	23

2.3 Chemical additions

Phosphorus was removed in the aqueous phase by chemical precipitation with $FeSO_4.7H_2O$ (iron (II) sulfate heptahydrate) and $FeCl_3$ (iron (III) chloride hexahydrate) added at three distinct dosing points. $FeSO_4$ was dosed in the pre-aeration tank before the primary clarifier and in the aerobic tank (BR4/AEROB), whereas $FeCl_3$ was added at the end of the post-denitrification (BR6/ANOX) before the MBRs. The addition of $FeSO_4$ to the pre-aeration was flow proportional with an annual average flow of 10 $gFe.m^{-3}$ while the addition of $FeSO_4$ in the BRA4/AEROB was controlled towards a set point of 0.2 $gP.m^{-3}$ in the treated effluent with a maximum dose of 15 $gFe.m^{-3}$. $FeCl_3$ added before the MBRs was also controlled towards a set point of 0.15 $gP.m^{-3}$ in the effluent with a maximum dose of 15 $gFe.m^{-3}$. Brenntaplus (a mixture of proteins, sugars and alcohols) was used as an external carbon source at a concentration of 1000,000 $gCOD.m^{-3}$. It was dosed in the post-anoxic tank (BR6/ANOX) and the dosage was controlled towards a preselected nitrate concentration (set point 3 $gN.m^{-3}$) in the effluent.

2.4 Wastewater characterisation

2.4.1 SCADA data

Daily data were obtained from the supervisory control and data acquisition (SCADA) system. Data acquisition included online flow rates of water and sludge streams and air to the activated sludge system, PO_4-P, NO_3-N on treated effluent, dissolved oxygen (DO), suspended solids (SS), temperature and pH in MBR 2.

2.4.2 Plant routine measurement data

Data from routine sampling and offline analysis were provided by SVOA for use in the model analysis. These included routine daily and weekly measurements on composite samples from auto-samplers located at the influent, primary effluent, effluent (treated outflow), bioreactor 4 and RAS/DEOX line. Analyses on the influent and effluent included total organic carbon (TOC), 7-day biological oxygen demand (BOD_7), total suspended solids (TSS), volatile suspended solids (VSS), total suspended solids (TSS), total dissolved solids (TDS), volatile fatty acid (VFA), ammonia (NH_4-N), nitrate (NO_3^-), total nitrogen (TN), phosphate (PO_4-P), total phosphorus (TP), alkalinity, soluble calcium (Ca), magnesium (Mg), sodium (Na) and potassium (K). Analyses were generally done using Standard Methods (APHA, 2012). The samples were conserved with 1 part 4M sulfuric acid to 100 parts sample

volume, except for samples tested for TOC, which were conserved with 2M hydrochloric acid in corresponding proportions. In addition to external analyses, other samples were analysed internally (onsite) for TSS, filtered and total COD, total nitrogen and ammonium nitrogen by colorimeter using a spectrophotometer (WTW Photolab 6600). Data collected over the period from 20 June 2016 to 10 April 2017 were selected and averaged before use as a representative measure of steady state conditions.

2.4.3 Intensive sampling and offline analysis

Intensive sampling and offline analyses were carried out to augment routine measurements at the plant. Grab and composite samples were collected daily for a week over the period 12/07/2017 to 19/07/2017 from five different points: influent, primary effluent, mixed liquor, effluent, from one of the bioreactors (BR4/AEROB) and RAS/DEOX return sludge. Samples were stored in a cooler box with ice bricks and transported to an external laboratory (Eurofins Environment Sweden AB), which conducted the analyses.

2.5 Plant-wide model configuration

2.5.1 Plant model configuration

The model was adapted from the Benchmark Simulation Model No. 2 (BSM2) (Gernaey *et al.*, 2014, Solon *et al.*, 2017). Briefly, the primary settling tank was modelled as one non-reactive settler (Otterpohl and Freund, 1992). Biological kinetics in the activated sludge plant were described by ASM2d (Henze *et al.*, 2000), expanded to include physico-chemical processes as described below (Solon *et al.*, 2017). Furthermore, the TSS in ASM2d was computed from volatile suspended solids (VSS) and inorganic suspended solids (ISS). The membranes were simply described as a reactive filtration system with wastewater entering at the bottom, permeate exiting at the top of the membranes and retained biomass leaving from the base to be recycled back to the activated sludge as returned activated sludge. Sludge thickening and dewatering units were assumed to be ideal (with constant split fraction and characteristics) with no hold-up volume (Jeppsson *et al.*, 2007).

Although the plant under study did not have a sludge treatment train, an anaerobic digester was set on the thickened sludge line. This allowed a full evaluation on the impacts of iron salts to be carried out in the pilot plant as a whole. Biochemical conversion processes in the anaerobic digester were described by the ADM1 (Batstone *et al.*, 2002), which was upgraded to include recent developments, such as physico-chemical and biological iron, sulphur and

phosphorus transformations (Flores-Alsina *et al.*, 2016). For a full explanation of the extended ADM1 model, as well as a detailed description on the matrix format used to represent anaerobic digestion model, the original publication (Batstone *et al.*, 2002; Solon *et al.,* 2017) should be consulted. To date, ASM and ADM1 have not been developed in a plant-wide context and, importantly, have not had a common state set (mainly due to complexity and simulation speed in single environment applications). For this reason, the ASM and ADM1 models have typically required state conversion interfaces. To connect ASM and ADM1, model interfaces were used to translate modelled state variables. The interfaces between the ASM – ADM1 and ADM1 – ASM2d were modelled based on continuity principles (Nopens *et al.*, 2009) Additional details about how ASM2d and ADM1 models were interfaced can be found in Solon *et al.* (2017).

The membrane bioreactor model consisted of two distinct sub-models that simulated biological and physical mechanisms simultaneously, taking into account the interactions between them. The first sub-model described the activated sludge processes, particularly ASM2d, which was modified to consider the influence of soluble microbial products (SMPs) consisting of the utilization-associated products (UAPs) and the biomass associated products (BAPs) (Jiang *et al.*, 2008). The second sub-model based on the membrane filtration simulated the relevant physical processes that take place in the MBR and that directly or indirectly influence the biological transformations. Membrane fouling was not taken into account to avoid potential model complexity due to a large amount of parameters to calibrate the fouling model. However, aeration was incorporated in the MBR model for fouling control so that its impact on the activated sludge treatment could be evaluated. Backwashing and relaxation were not physically modelled.

2.5.2 Physico-chemical model

The physico-chemical model consisted of two parts; an algebraic equation set for aqueous-phase reactions (weak acid-base and ion-pair equilibrium) and rate expressions for minerals precipitation, minerals dissolution and gas transfer (Kazadi Mbamba *et al.*, 2015a; b).

a*) Chemical equilibrium and ion pairing*

Weak acid-base reactions and ion pairing were mathematically described with a set of non-linear algebraic equations, which included one law mass-action for each aqueous phase

reaction and a number of molar contribution balances to satisfy the required degrees of freedom for the calculation. In general form, the mass action laws are:

$$a_i = K_i \prod_{j=1}^{N} a_j^{v_{ij}} \qquad i = 1,2 \ldots, N \tag{1}$$

where a_i is an iterative species expressed in terms of chemical activities, a_j is the activity of an ion pair, K_i is the equilibrium constant for aqueous phase reaction i, $v_{i,j}$ is the stoichiometric coefficient of the reactant or product j for aqueous phase reaction i. For a typical wastewater, 20 universal iterative species (Ac^-, Al^{3+}, Bu^-, CO_3^{2-}, Ca^{+2}, Cl^-, Fe^{2+}, Fe^{3+}, H^+, HS^-, K^+, Mg^{2+}, NH_4^+, NO_2^-, NO_3^-, Na^+, PO_4^{3-}, Pro^-, SO_4^{2-}, Va^-) and 118 species (ion pairs) were identified and included in the speciation model.

In general form, the molar contribution balances are:

$$TOT_j = Z_j + \sum_{i=1}^{N} v_{ij} Z_i \quad j = 1, 2 \ldots, N \tag{2}$$

where TOT_j is the total measurable concentration of an aqueous phase ingredient, which is the sum contribution of that ingredient in various chemical forms in the aqueous phase. Z_j is the concentration of an iterative species and Z_i is the concentration of an ion pair. Activity coefficients (γ_j or γ_i) were determined from the Davies approximation with temperature correction, and equilibrium constants (K_i) were also corrected for temperature using the constant-enthalpy form of the van't Hoff equation (Stumm and Morgan, 1996; Flores Alsina *et al*., 2015; Gustafsson, 2015).

b) Chemical precipitation model

The activated sludge system model was extended with the chemical precipitation processes of two minerals, namely hydrous ferric oxide (HFO) and iron phosphate ($FePO_4$). The theory of coagulation and chemical precipitation reactions is very complex. A greatly simplified and general scheme of chemical P removal involving processes, such iron oxidation-reduction, precipitation and adsorption on HFO surfaces, is illustrated in Figure 2. Removal of P by chemical precipitation and sorption were assumed to take place in parallel and therefore be competing for soluble ferric iron ions in the wastewater within the bioreactors (Wu *et al.*, 2015).

Firstly, iron transformations was described using the hydrous ferric oxide model, which describes how the precipitation of freshly formed and highly reactive HFO provides a number

of adsorption sites for ions on its surface (Hauduc *et al.*, 2015). However, a simplified HFO model was used (Solon *et al*., 2017). Briefly, the HFO model describes the precipitation of amorphous iron hydroxide or HFO, phosphate adsorption/binding onto X_{HFO} (HFO particulates) and their ageing as the crystallinity increases. HFO initially precipitates with a high adsorption capacity, which has an open structure and easily accessible binding sites. Through aging process, it loses reactivity and has a more compact structure and less accessible sites. Adsorption of phosphates onto HFO leads to production of HFO with bounded phosphates ($X_{HFO,H,\ P}$ and $X_{HFO,L,P}$). Because of increased probability of floc breakages for older HFO, the kinetic rate of aging is assumed to be higher for $X_{HFO,H}$ than for $X_{HFO,L}$.

Gas transfer included O_2 and CO_2 in ASM2d and CO_2, NH_3, H_2O and CH_4 in the ADM1, all of which were modelled as single-film mass transfer controlled processes (Batstone *et al.*, 2002).

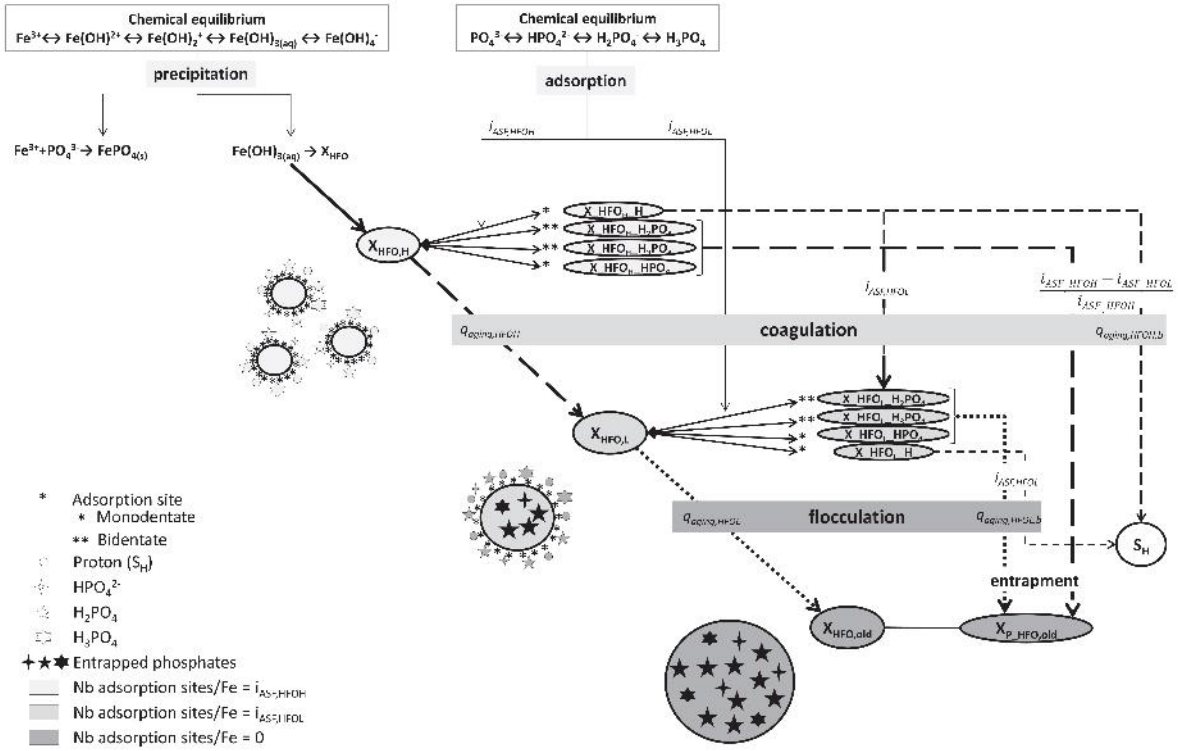

Figure 2 *– The chemical phosphorus removal model included in the extended ASM2d (chemical precipitation and phosphorus adsorption and co-precipitation) (Hauduc et al., 2015).*

When iron salts, such as $FeSO_4$, are added to the aerobic tank, Fe^{2+} will undergo oxidation into ferric iron as follows:

$$Fe^{2+} + ¼\ O_2 + H^+ \rightarrow Fe^{3+} + ½\ H_2O \quad (3)$$

The reaction consumes a stoichiometric amount of 0.14 g O_2/g Fe^{2+}. The oxidation of dissolved ferrous iron leads to the formation of amorphous to poorly crystalline ferric-precipitates with a very high sorption capacity for phosphorus. HFO precipitates, formed by oxidation of Fe^{2+} in the mixed liquor, will affect the removal of P by adsorption and co-precipitation.

Secondly, iron phosphate precipitation (X_{FePO4}) was described as a reversible process using the supersaturation as the chemical driving force. The rate expression for iron phosphate (strengite) precipitation rate was (Kazadi Mbamba *et al.*, 2015b):

$$r_{FePO4} = k_{FePO4} X_{FePO4} \sigma^n \quad (4)$$

where r_{FePO4} is the iron phosphate precipitation rate (gFe.m^{-3}.d^{-1}), k_{FePO4} is an empirical kinetic rate coefficient (d^{-1}), X_{FePO4} (gFe.m^{-3}) is the concentration of precipitate at any time *t* (a dynamic state variable). *n* is the order of the precipitation reaction (equal to 2 for iron phosphate) with respect to supersaturation, calculated as follows for iron phosphate as an example:

$$\sigma = \left(\frac{Z_{(Fe^{3+})}{}^{x}\ Z_{(PO_4^{3-})}}{Ksp_{FePO4}} \right)^2 - 1 \quad (5)$$

where $Z_{(Fe3+)}$ and $Z_{(PO43-)}$ are the chemical activities of ferric iron and phosphate ions in the aqueous phase and $K_{SP,FePO4}$ is the solubility product constant for iron phosphate.

In the extended ADM1, mineral precipitation is also described as a reversible process using supersaturation as the chemical driving force. The multiple minerals in ADM1 include calcite, aragonite, amorphous calcium phosphate and struvite. Furthermore, the extension of ADM1 includes iron phase transformation. Ferric iron in the form of hydrous ferric oxides ($X_{HFO,L}$, $X_{HFO,H}$) undergoes reduction to ferrous iron using hydrogen and sulfide as electron donor (Solon *et al.*, 2017). Once released Fe^{2+} can preferentially bind with S^{2-} to form iron sulphide. Additionally, Fe^{2+} in excess may also combine with soluble phosphate present in

the anaerobic digester to form vivianite ($Fe_3(PO_4)_2$). $FePO_4$, if undersaturated, may undergo dissolution releasing Fe^{3+} and soluble P.

2.5.3 Influent COD fractionation modelling

The fractionation of COD in the influent was performed using the routine data provided by the pilot plant operator. The organic matter in the influent was fractionated into fermentable, readily biodegradable organic compounds (S_F), fermentation products (S_A), inert soluble organic compounds (S_I), slowly biodegradable organic compounds (X_S) and inert particular organic compounds (X_I) (Henze *et al.*, 1995). Briefly, the biodegradable COD ($S_F + S_A + X_S$) concentration was estimated based on BOD_7 test data made available by the plant operator and using the method as described by Grady Jr *et al.* (2011). Fermentation products (S_A) were estimated to be equal to measured VFAs. Readily biodegradable COD ($S_F + S_A$) was estimated using the floc/filtration procedure proposed by Mamais *et al.* (1993), based on the assumption that suspended solids and colloidal particulates are captured and removed by flocculation with a zinc hydroxide precipitate to leave only truly dissolved organic matter after filtration. 90% of the soluble COD measured in secondary effluent samples was assumed to be non-biodegradable soluble COD (S_I) (Siegrist and Tschui, 1992).

The values of influent variables, such as total suspended solids (X_{TSS}), total dissolved ammonia nitrogen (S_{NH4}), nitrate (S_{NO3}) and inorganic soluble phosphorus (S_{PO4}), were assumed to be equal to experimentally measured values (average measured for weekly composite samples). Other variables in the influent, such as dissolved oxygen (S_{O2}) and dinitrogen (S_{N2}), were set to zero. Particulate components, namely nitrifying organisms (X_{AUT}) and heterotrophic organisms (X_H) were assumed to be negligible in the influent as per Henze *et al.* (1995). Since phosphorus was removed chemically, all the bio-P processes were deactivated in ASM2d and therefore, phosphate-accumulating organisms (X_{PAO}), polyphosphates (X_{PP}) and poly-hydroxy-alkanoates (X_{PHA}) were assumed to be equal to zero in this study.

2.5.4 Synthetic (long-term) influent data generation

The static influent characteristics obtained from the analysis above, were used to estimate dynamic influent base characteristics. A simplified dynamic influent generator was used to re-create long-term dynamics (Gernaey *et al.*, 2011). Since data related to influent wet weather flow-rate conditions were missing for the pilot-system, the measured flow rate data

were used. A temperature module was not included in the model since the measured data were available and used instead. Finally, an additional module had to be included in order to capture the dynamics of cations (Na, K, Ca, Mg) and anions (Cl). The influent generator results were validated against a corresponding dataset for a subset of influent characteristics.

2.6 Model implementation

The combined biological and physico-chemical models together form a differential-algebraic equation set, which was implemented as Matlab C-MEX files and was solved in MATLAB/SIMULINK (Version 8.1, Mathworks Inc., USA) as described elsewhere (Gernaey *et al.*, 2014; Kazadi Mbamba *et al.*, 2016; Flores-Alsina *et al.*, 2015; Solon *et al.*, 2017).

2.7 Parameters

A systematic step-wise calibration procedure was performed in which a few kinetic parameters were adjusted to minimize discrepancies between the model output and static measured data from the pilot-plant (Kazadi Mbamba *et al.,* 2016). With the exception of the influent characterisation, model parameters for ASM2d and ADM1 were kept at default values (Henze *et al.*, 2000; Batstone *et al.*, 2002). The autotrophic saturation coefficient for phosphorus in growth was reduced from 0.01 to 0.001 $gP.m^{-3}$ due to lower concentration of PO_4 that could be reached in the bioreactors as a result of chemical treatment. The Davies approximation to activity coefficients was used with temperature correction, and equilibrium constants were also adjusted for temperature using the constant-enthalpy form of the van't Hoff equation (Stumm and Morgan, 1996). For minerals precipitation reactions in the anaerobic digester, precipitation rate coefficients (k_{cryst}) estimated in a previous study were used (Kazadi Mbamba *et al.*, 2015b).

The default parameter values defined in BSM2 were first used for the primary clarification model (Gernaey *et al.*, 2014). However, the use of these values overestimated the efficiency performance. So, based on empirical knowledge, the efficiency correction factor was altered from 0.65 to 0.3 in the primary clarifier model and the WAS flow was adjusted accordingly to change the concentrations of suspended solids in the RAS and mixed liquor to observed values of 6,500 $g.m^{-3}$ and 8,500 $g.m^{-3}$, respectively.

2.8 Model scenarios

Scenario analyses were used to investigate the performance of the plant-wide model and the impact of simultaneous precipitation on phosphorus removal under steady-state and dynamic conditions. The criteria that were used to assess model performance were effluent quality in the water line including soluble ammonia nitrogen, nitrate and phosphate. The following five scenarios were selected for model evaluation:

i) Scenario 1 (*Base case)* – plant-wide model with MBR, chemical precipitation, closed loops for DO in the aerobic zones and NO_3 in the post-anoxic zone were implemented. The DO concentrations in the aerobic tanks were controlled towards a set point of 2.0 $g.m^{-3}$ by manipulating the air supply rate, while an external carbon was added to the pre-anoxic tank to maintain the concentration of NO_3 at 3 $gN.m^{-3}$.

ii) Scenario 2 *with changed concentration of* $FeSO_4$. This scenario was designed to assess the (response) time constant under dynamic conditions when the concentration of iron salts change and how this will affect the phosphorus removal.

iii) Scenario 3 *with phosphorus controller*. The base case was simulated as in Scenario 1 except that dosing of Fe salts was controlled towards a predefined concentration of phosphorus in the effluent by manipulating the metal flow rates ($FeSO_4$ or $FeCl_3$). This scenario examined whether inclusion of a phosphorus controller in chemical precipitation would be essential to achieve low P effluent while at the same time avoiding too low P concentrations, which is detrimental to biological processes in the bioreactors.

iv) Scenarios 4, 5 & 6 were designed to investigate the impact of changing the location of dosing of iron sulphate fed to the activated sludge system. During this simulation analysis, the iron sulphate additions were varied between three different reactors: aerobic, anoxic and DEOX/RAS.

The different scenarios above were analysed based on 294 days of simulation with dynamic influent conditions. To ensure that the model had reached steady-state before beginning the analysis, a simulation was run for at least 300 days with a static influent and results at the end of this simulation was reused as initial values for the dynamic simulations.

3 Results and discussion

3.1 Steady-state plant influent

Due to unavailable data necessary for influent characterization and COD fractionation, old data from 2015 were used to fractionate COD and calculate the COD ratios, which were kept constant with regard to the 2016-2017 data used in the steady-state simulations. These ratios were also assumed constant and applied in the phenomenological model to derive the ASM2d dynamic state variables as presented in the next section. Table 4 shows the measured total, filtered and flocculated COD data as well as the different COD fractions for the old data. The readily biodegradable and fermentation products fractions accounted for 13% and 9% of the total COD, respectively. The slowly biodegradable fraction had the highest percentage (56% of total COD), while the non-biodegradable organics and the heterotroph biomass were 11% and 6%, respectively. The non-biodegradable fraction was used as one of the calibration parameters for the sludge age in the activated sludge system; however, this step was outweighed by the adjustment of the primary clarifier efficiency, which affected the amount of particulates entering the activated sludge system.

Table 4 *– Measured total, filtrated and flocculated COD as well as calculated COD fractions.*

Parameters	**COD ($g.m^{-3}$)**	**COD ratio**
COD	466±42	1
Soluble COD	174±9	0.4
Flocculated COD	122±9	0.26
Readily biodegradable, S_F	60	0.13
Fermentation products, S_A	40	0.09
Inert biodegradable organics, S_I	22	0.05
Non-biodegradable organics, X_I	61	0.11
Slowly biodegradable substrate, X_S	245	0.56
Heterotrophic biomass, X_H	38	0.06
Autotrophic biomass, X_{AUT}	0	0

The averaged influent measurements and modelled influent composition for the pilot plant are presented in Tables 5 and 6, respectively. The pilot plant have only partly COD data available and the total organic carbon measurements were converted to COD using an observed ratio COD/TOC of 3.5. The plant had medium influent levels of organic matter (148 gTOC.m^{-3}; 521 gCOD.m^{-3}) and nutrients, such as ammonia nitrogen (39.1±1.7 gN.m^{-3}), and orthophosphorus (3.3±0.36 gP.m^{-3}). The influent contained 6.23 g.m^{-3} of total phosphorus, of which about 53% was soluble phosphorus and the remainder was particulate organic phosphorus. Total nitrogen was higher than ammonia (76% of TN), as is normal. The raw wastewater influent contained 249 gTSS.m^{-3} of total suspended solids (TSS).

Table 5 *– Average steady-state influent composition of the pilot-scale WWTP used for influent characterization.*

Parameters	**Measurements**
Total COD (gCOD.m^{-3})	521
Soluble COD (gCOD.m^{-3})	174
Flocculated COD (gCOD.m^{-3})	137
BOD_7 (gCOD.m^{-3})	234
TN (gN.m^{-3})	48
Ammonium, NH_4 (gN.m^{-3})	37
Nitrate, NO_x (gN.m^{-3})	0.12
Phosphorus, Ptot (gP.m^{-3})	6.23
Orthophosphorus (gP.m^{-3})	3.3
Total organic carbon, TOC (g.m^{-3})	141
Total inorganic carbon, TIC (g.m^{-3})	75
Total suspended solids, TSS (gTSS.m^{-3})	249
Volatile suspended solids, VSS (gVSS.m^{-3})	223
VFA (gCOD.m^{-3})	40

Using the COD ratio described above, the organic matter contained an estimated significant quantity of soluble COD (174 gCOD.m^{-3}) including VFAs (40 gCOD.m^{-3}). The results of the

characterization showed a low (0.15) ratio between the readily biodegradable and slowly biodegradable substrates. The ratio of inert organic material to the slowly biodegradable substrate was 0.15. These fractions did not change very much after the primary clarifier, which was performing very poorly with a removal efficiency of less than 30%.

Table 6 *– Average steady-state influent composition of the pilot-scale WWTP used for influent steady state model validation. COD ratios determined previously was used in the influent composition.*

Model influent composition (ASM2d variables)	**Values**
Dissolved oxygen, SO_2 ($g.m^{-3}$)	0
Readily biodegradable, S_F ($gCOD.m^{-3}$)	67
Fermentation products (acetate), S_A ($gCOD.m^{-3}$)	45
Ammonium, S_{NH4} ($gN.m^{-3}$)	37
Nitrate (plus nitrite), S_{NO3} ($gN.m^{-3}$)	0.12
Phosphate, S_{PO4} ($gP.m^{-3}$)	3.3
Inorganic carbon, S_{IC} ($gC.m^{-3}$)	75
Inert biodegradable organics, S_I ($gCOD.m^{-3}$)	25
Inert, non-biodegradable organics, X_I ($gCOD.m^{-3}$)	47
Slowly biodegradable substrate, X_S ($gCOD.m^{-3}$)	314
Heterotrophic biomass, X_H ($gCOD.m^{-3}$)	24
Suspended solid, X_{TSS} ($gCOD.m^{-3}$)	249

3.2 Dynamic plant influent

The purpose of fitting BSM2 influent generator model to full-scale plant data was to provide a representative input for dynamic simulation analyses. Figure 3 shows a representative full-scale data set over 294 days together with the influent generator model simulations for flow rate, COD, ammonia nitrogen and soluble phosphate starting from June 2016 to April 2017. The influent generator provided modelled data at 5 min intervals, whereas actual measurements were relatively sparse with only daily or weekly sampling and analysis. Rainfall patterns were not included in the model due to limited data, but existing measurements of influent flow rate with an annual average of 71 $m^3.d^{-1}$ were used instead.

Figure 3 also shows that there was a reasonable good agreement between measured and simulated concentrations of ammonia nitrogen, phosphate, COD and TSS. Similar to the influent flow rates, the measured temperature data in the pilot-test were used for the dynamic simulations.

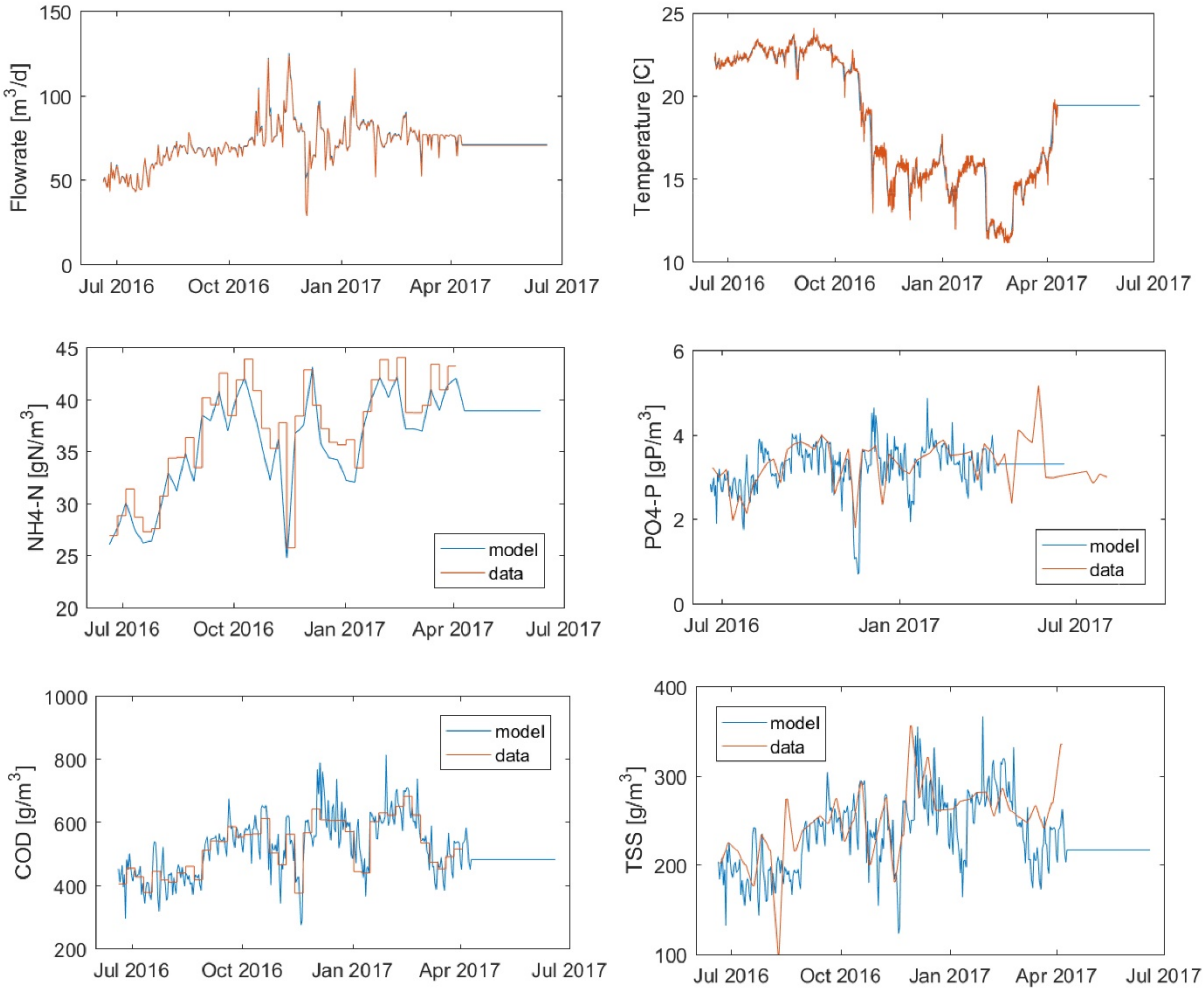

Figure 3 *– Dynamic plant influent for representative measured and simulation data. The blue and red solid lines represent the measured and simulated results, respectively.*

3.3 Plant steady-state response

3.3.1 Model calibration

As indicated above, phosphorus was removed from wastewater by chemical precipitation with $FeSO_4$ and $FeCl_3$ added at three distinct location points. While $FeSO_4$ was dosed in the pre-aeration tank before the primary clarifier and in the aerobic tank, $FeCl_3$ was added at the end of the post-denitrification before the MBRs. Figure 4 presents the modelled steady state

and average measured data for key variables. With the parameter adjustments of solids separation and nitrification parameters including the saturation coefficient for phosphorus in growth, it was possible to obtain reasonable agreement between modelled and measured TSS, soluble phosphorus and ammonia in the different streams. The model was able to predict the concentration of P in the effluent. For the steady-state scenario, differences between measured and modelled phosphorus of 5-10% was observed throughout the pilot plant and the prediction error for ammonia nitrogen was below 1%. The relative error for measured and predicted suspended solids (SS) in the primary effluent, mixed liquor and return activated sludge was 3%, 1% and 6%, respectively. However, significant SS differences were seen in the effluent likely due to faulty SS meters in the pilot plant, whereas the model assumes ideally a complete retention of solids the membranes.

The total iron concentration was low in the effluent indicating that almost all of the added iron salts precipitated out of the mixed liquor and was incorporated in the activated sludge. Available data required for the precipitation model related to iron speciation were limited, nevertheless pilot plant performance with respect to total iron was predicted very reasonably. Given the low concentration of total Fe in the effluent, it can be assumed that dosing $FeCl_3$ at the membranes provided additional removal of P with no evidence of short-circuiting. As such, a large amount of iron minerals in the form of HFO (about 70% of iron precipitates) and iron phosphate (approximately 30% of iron precipitates) was retained in the activated sludge within the bioreactors with this mechanism most likely accounting for phosphorus removal. The proportion of HFO/$FePO_4$ will significantly vary depending on a number of operational factors including the pH, Fe/P ratio, the oxidation of Fe^{2+} to Fe^{3+} as well as the equilibrium concentrations of ferric iron and soluble phosphate. These factors including the sludge age are vital when assessing control strategies with respect to efficient removal of phosphorus. While data related to Fe^{2+} and Fe^{3+} species were unavailable, a literature review shows that ferrous iron added to an oxidizing environment converts to ferric iron, which is then participated in P removal via the precipitation or adsorption pathways (Wang et al, 2014). Dosing Fe^{3+} is preferable since the oxidation step is avoided; however, the cost of ferric salts is higher compared to ferrous salts, such as $FeSO_4$. Iron speciation is key in studying Fe chemistry and will therefore increase understanding of chemical P removal mechanism.

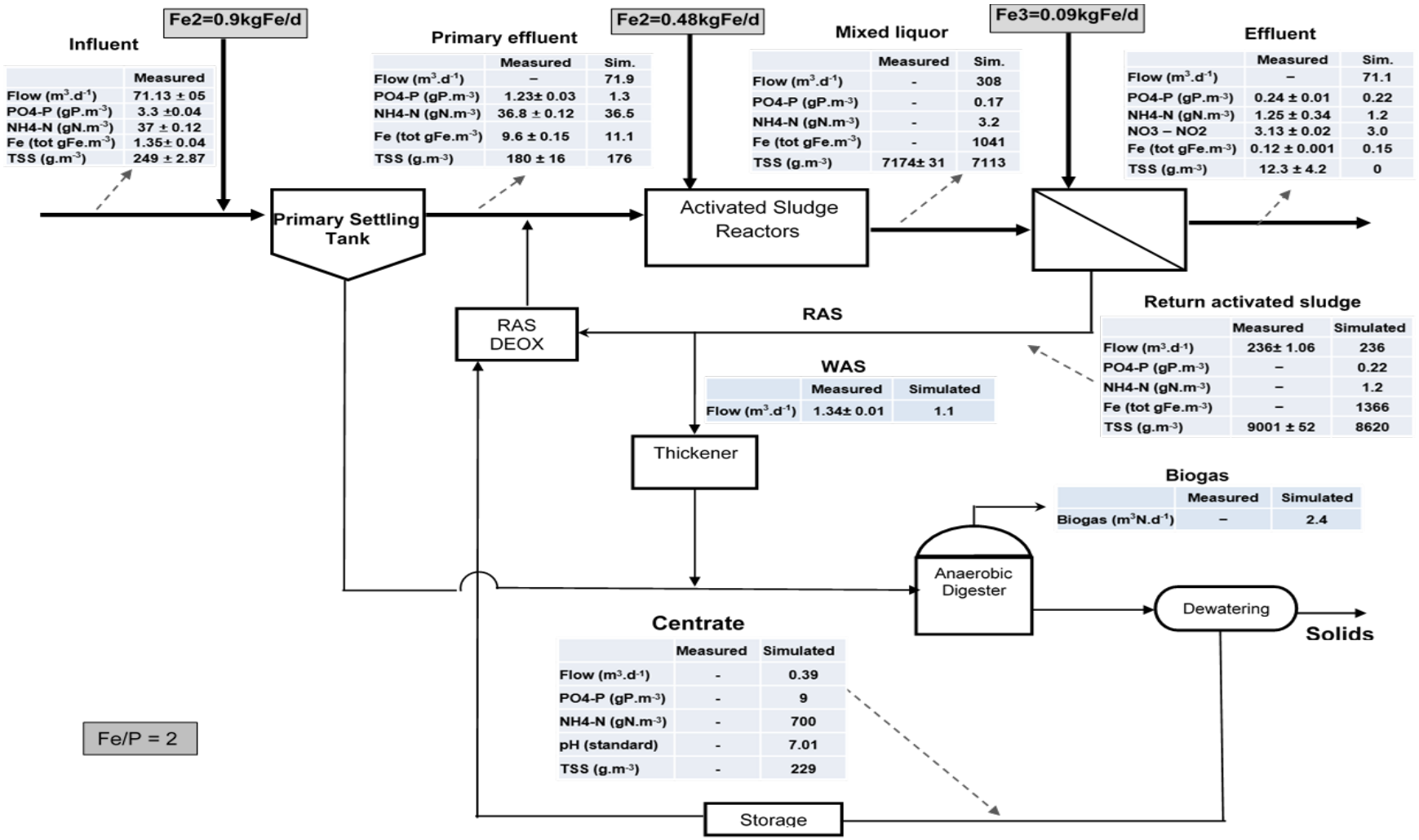

Figure 4 *– Steady-state comparison between the model prediction and measured data for representative streams and variables across the pilot treatment plant. $FePO_4$ was added in a pre-aeration tank (before primary settling tank, not shown) and in the first aerobic tank, $FeCl_3$ was added before the MBRs.*

The model simulated biogas production at 2.4 m3.d-1, which is lower probably due to a low sedimentation efficiency in the primary clarifier (less than 30%). However, experimental data were not available to evaluate the prediction accuracy since a sludge treatment facility at the pilot plant was underway.

3.3.2 Impact of pH and Fe/P molar ratio

The calibrated plant-wide model was used to carry out further simulations to study the impact of pH and molar ratio of Fe/P on the removal efficiency of phosphorus. The pH was varied between 6.7 to 7.4 by changing the amount of sodium hydroxide in the influent whereas the Fe/P ratio was varied by increasing proportionally the amount of iron salts added at all three dosing points. Other parameters of the system's phosphorus removal remained approximately the same. As shown in Figure 5, the effluent P concentration significantly decreased with decreasing pH at higher molar ratio between Fe and P. For example for the lowest ratio (Fe/P=1), the effluent P dropped from 0.62 $gP.m^{-3}$ at higher pH (7.4) to 0.1 at pH 6.7. This shows that the pH and the molar ratio of iron to the phosphorus concentrations affect the competition between hydroxyl ions and phosphates for ferric ions at the point of addition, thus the fractions of HFO minerals and $FePO_4$. These results are in good agreement with other studies (Hauduc et al, 2016), except that the pH variation in the simulations has been limited within the range in wastewater treatment. In general, the pH of a wastewater affects chemical species distribution of the weak acid-base systems, such as phosphate, which in turn dictate simultaneous chemical precipitation. $FePO_4$ is likely to be the dominant phosphate precipitate at low pH levels (6.5-6.7) due to increased levels of orthophosphate, whereas P sorption of HFO surfaces appears to be the main removal mechanism affecting the fate and transport of phosphorus at higher pH (from pH 6.7 and above). However, the relative differences of P concentrations in the effluent between the highest and lowest Fe/P ratios was higher (0.25) at higher pH but became smaller (0.06) at lower pH indicating that increasing the concentrations of iron salts would not translate in further removal of phosphorus when the residual P concentration is very low. This is in agreement with other studies, which have reported that the efficiency of dosing chemicals drops significantly at low effluent phosphorus concentrations (De Haas *et al.*, 2000a, b, 2001).

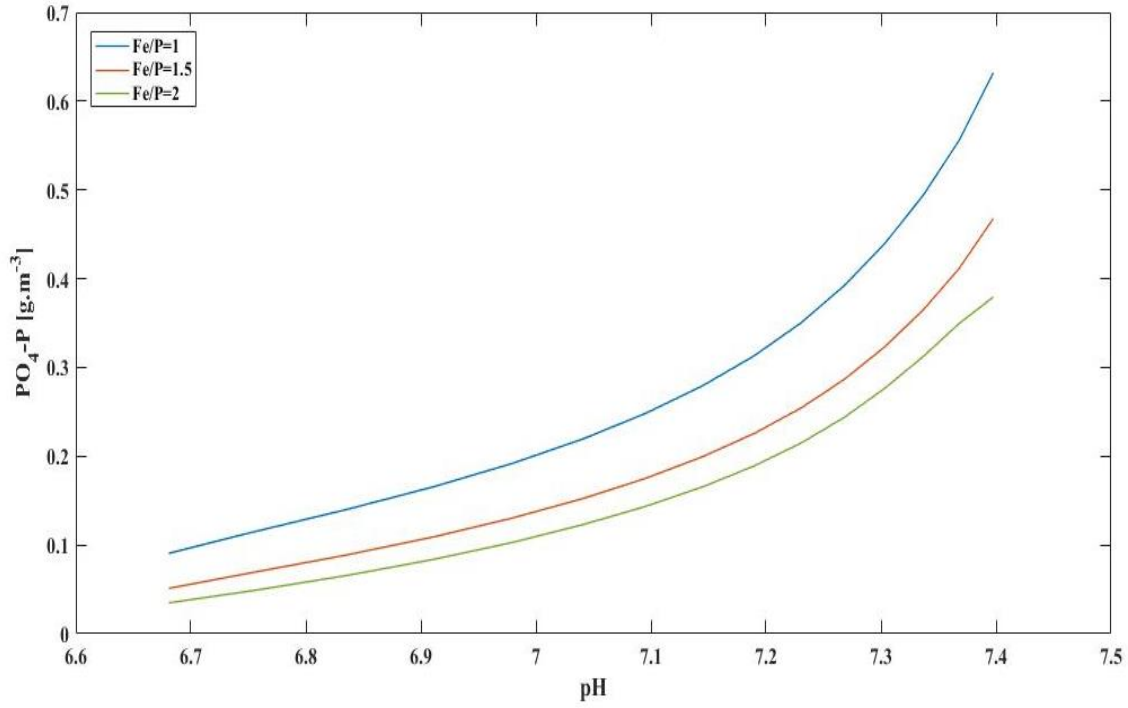

Figure 5 *– The impact of pH and Fe/P molar ratio on the dissolved phosphorus in the effluent.*

3.3.3 Time constant of chemical precipitation

Step change simulations were carried out making use of the calibrated plant-wide model to determine the time constant of the chemical precipitation process. The time constant was determined as the time required by the effluent P to reach 63.2% (from a $FeSO_4$ step decrease) or 36.8% (from a $FeSO_4$ step increase) of its total change. Figure 6 presents the results of the step changes. The time constants were found to be 5.25 d and 5 d when the flow rate was decreased and increased by 10%, respectively. This indicates that when the dosing of $FeSO_4$ is changed in the wastewater treatment system, the effluent P will also vary accordingly. The $FeSO_4$ dosing has a direct and large effect on the effluent P, but with slow dynamics. The change seems to be the largest in the beginning and eventually the effluent P will approach a new equilibrium state at least in 5 days. The cause of the delay may be due to dissolution, oxidation, formation, growth and aging of HFO complexes. The idea of feedback control of a slow-responding process will be to adjust the dosage of precipitants such that the effluent P is kept as close as possible within the acceptable operating region, in spite of process disturbances.

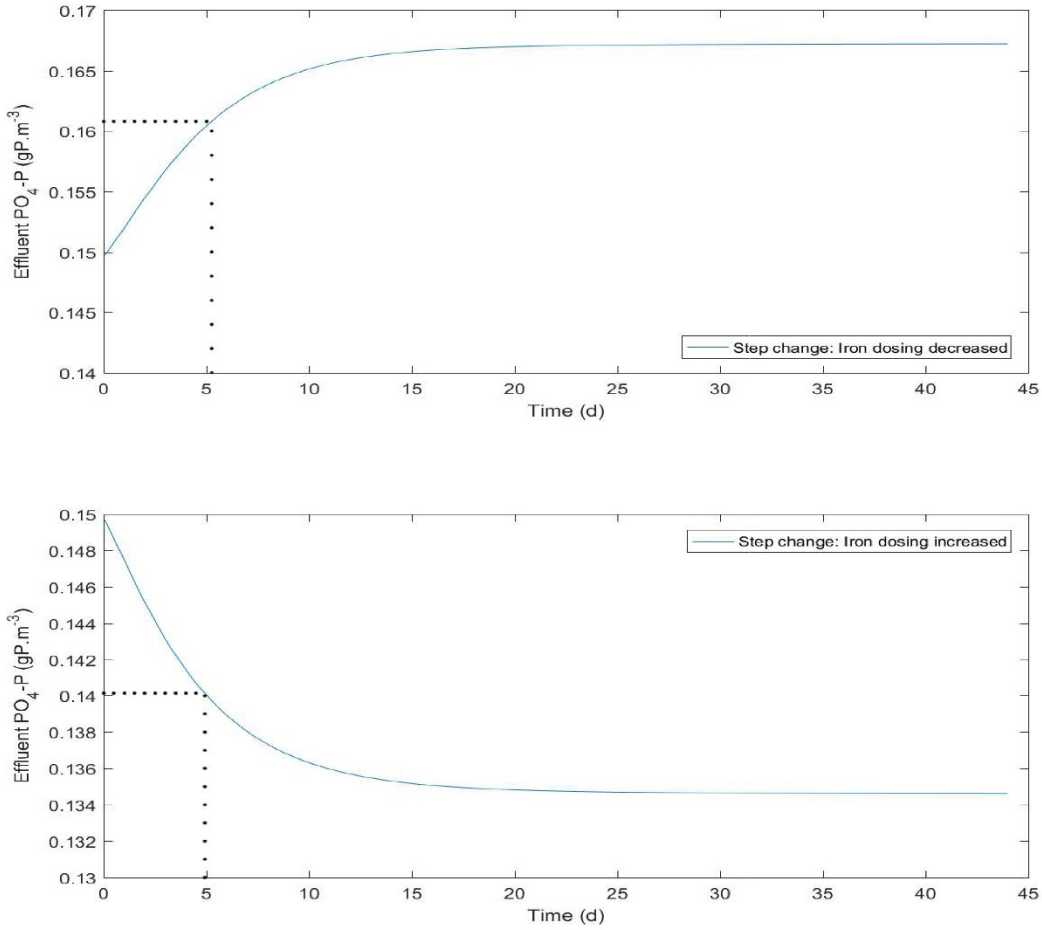

Figure 6 – *Dynamic response in effluent P to step change in iron salt ($FeSO_4$) dosage decrease (a) and increase (b).*

Similarly, the experimental investigations at the pilot plant under study showed a slow response when the dosed amount of precipitants was changed, and therefore corroborate with these simulations. The current behaviour in the pilot plant and the simulations possibly indicates a persistence effect of the dosed iron being recycled in the sludge and to continue removing phosphorus even after reducing/stopping the chemical dosing. A likely explanation for this effect is that the chemical phosphorus removal can take place by two simultaneous and competing reactions: a reaction of phosphate and HFO (by adsorption and co-precipitation) as well as a possible rapid direct iron phosphate precipitation (at the point of addition) (Wu *et al*., 2015). Freshly formed HFO and possibly (amorphous) iron phosphate in the wastewater are potentially highly reactive (high surface areas or binding sites) and are able to partake in the removal of phosphorus from wastewater. However, their reactivity deteriorates through aging, which occurs as the minerals accumulate in the bioreactors while being recycled as part of the return activated sludge. This indicates that the accumulation of

the Fe precipitates appears to contribute to more efficient phosphorus removal. The implication of this assertion is that the solid retention time (SRT) plays a critical role in determining the effluent P concentration. In other words, during simultaneous precipitation, iron dosed directly to the bioreactors or membrane tanks within the MBR system where sludge recycling is taking place with much longer SRTs (23 days) will participate in P removal. Additionally, the effluent P will decrease with increasing SRT indicating that the sludge age is one of the key operational parameters controlling the iron sludge content in the bioreactors and influences both the P in the effluent and eventually the MBR characteristics. On the other hand, a higher SRT would involve more old sludge (less reactive), however HFO reactivity is apparently maintained as iron, cycling in the MBR system, undergo reduction-oxidation reactions while alternating between anoxic and aerobic conditions (Bligh et *al.*, 2017).

3.4 Analysis of model variants

3.4.1 Plant-wide dynamic response

In order to demonstrate the application of the plant-wide model, several scenarios were considered in which effluent phosphorus qualities around 0.15-2 gP.m-3 were obtained using a stoichiometric molar ratio Fe/P = 2 with respect to the influent concentration. The effect of increasing or decreasing the amount of dosed chemicals was investigated as part of scenario 2. The dosing chemicals ($FeSO_4$ and $FeCl_3$) were fed directly to the aerobic tank and membrane tanks, respectively; their concentrations were decreased by 10% after 120 days while the plant was operated under dynamic conditions. Dosing $FeSO_4$ to the aerobic tank led to the oxidation of Fe^{3+}, which played a key role in removing P. Figure 7 shows the results of concentration profiles of phosphorus in the secondary effluent for the first three scenarios, which are also compared the total phosphorus in the influent (Figure 7a). The simulation results indicate that the concentrations of phosphorus in the effluent increase by approximately 44% for the 2nd scenario and decrease by 15% for the 3rd scenario, respectively. The increase of phosphorus in the effluent in the second scenario is due to the decreased contribution of the iron salt flows to the aerobic tank and MBRs. Figure 8 displays the total amounts of iron salt dosed at the three dosing locations to remove phosphorus from the influent. The striking feature in controlling PO_4 in the effluent is that the total amount of added iron was reduced by 18% from 1046 $gFe.d^{-1}$ in Scenario 1 (PO_4 open loop) to 889 $gFe.d^{-1}$ in Scenario 3 (PO_4 closed loop). It is worthwhile to mention that about 8.9% of iron

dosed in the first scenario was added as Fe(III) while the remaining (91.1%) was dosed as $FeSO_4$. The overall amount of Fe(III) was 8.6% in the second scenario, however it increased significantly to 44.6% in Scenario 3 (see Section 3.4.2 for further discussion).

Scenario 2 was carried out to simulate the behaviour of the pilot plant when the $FeSO_4$ dosage is increased or decreased and take corrective measures to ensure that the effluent quality is maintained. For example, after a period of limited dosage due to incorrect concentration precipitation chemicals, the modelling results show that this condition could be compensated for by increasing or decreasing Fe salt dosage. As indicated above, this result is in close agreement with observations at the pilot scale system under study, which showed a slow response of effluent P when iron dosing was interrupted. The slow kinetics observed in the pilot-test could indicate that the removal of phosphorus is not carried out by freshly added ferrous or ferric iron, but rather by growing and aging iron-precipitates in the sludge. As indicated above, redox cycling of iron in an MBR system is expected to maintain or reduce the rate of HFO reactivity loss as a result of reduction in anoxic zones and oxidation in aerobic zones (Blight *et al*., 2017). To this end, the presence of the accumulated precipitates has a beneficial effect on phosphorus and appears to be the major mechanism possibly due to the enhanced contact provided by the accumulated sludge, which lead to removal of P by adsorption or co-precipitation. Thus, the amount and reactivity of existing minerals present in the activated are indeed among the most influential factors for simultaneous precipitation reactions.

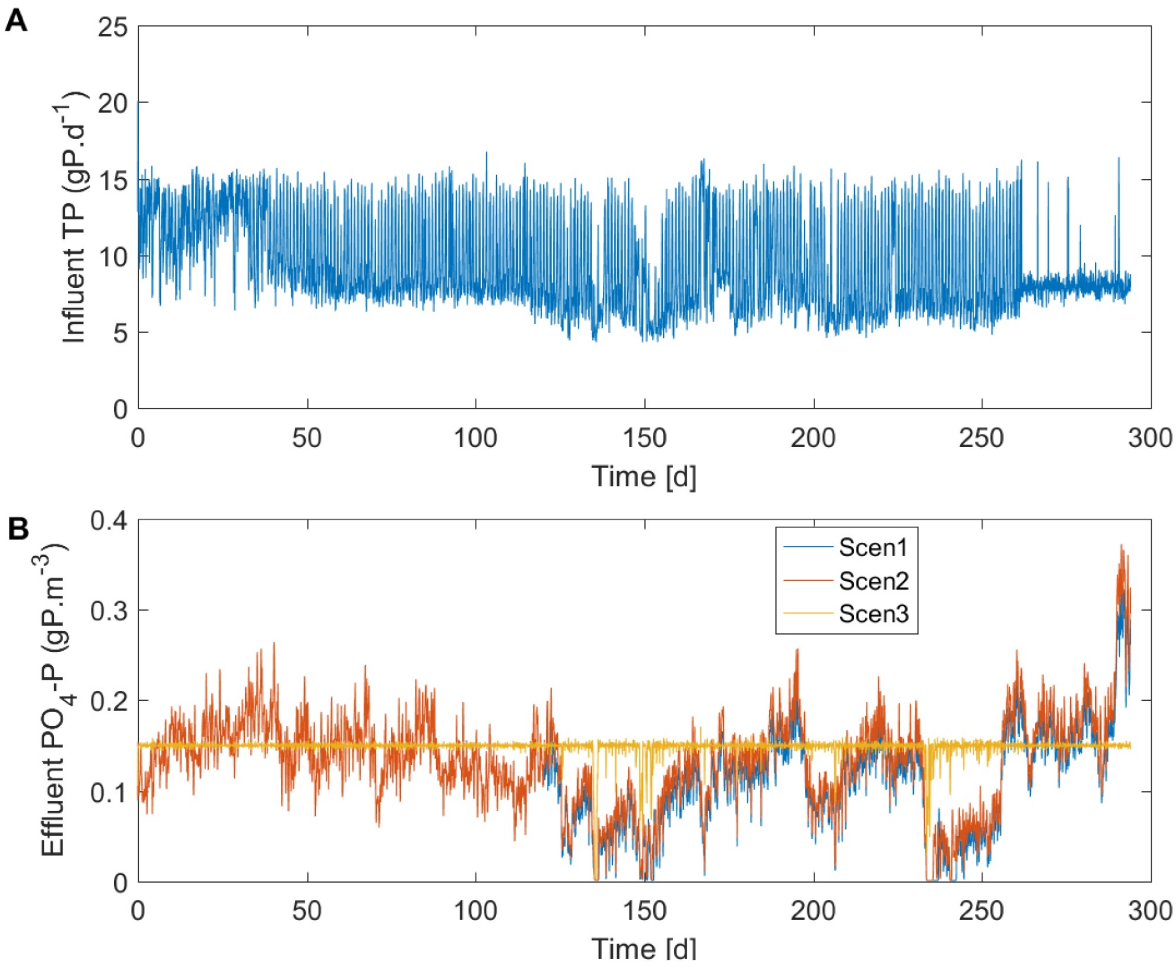

Figure 7 *– Total phosphorus in the influent and dynamic simulations of the soluble phosphate in the treatment plant outflow for Scenarios 1 - 3.*

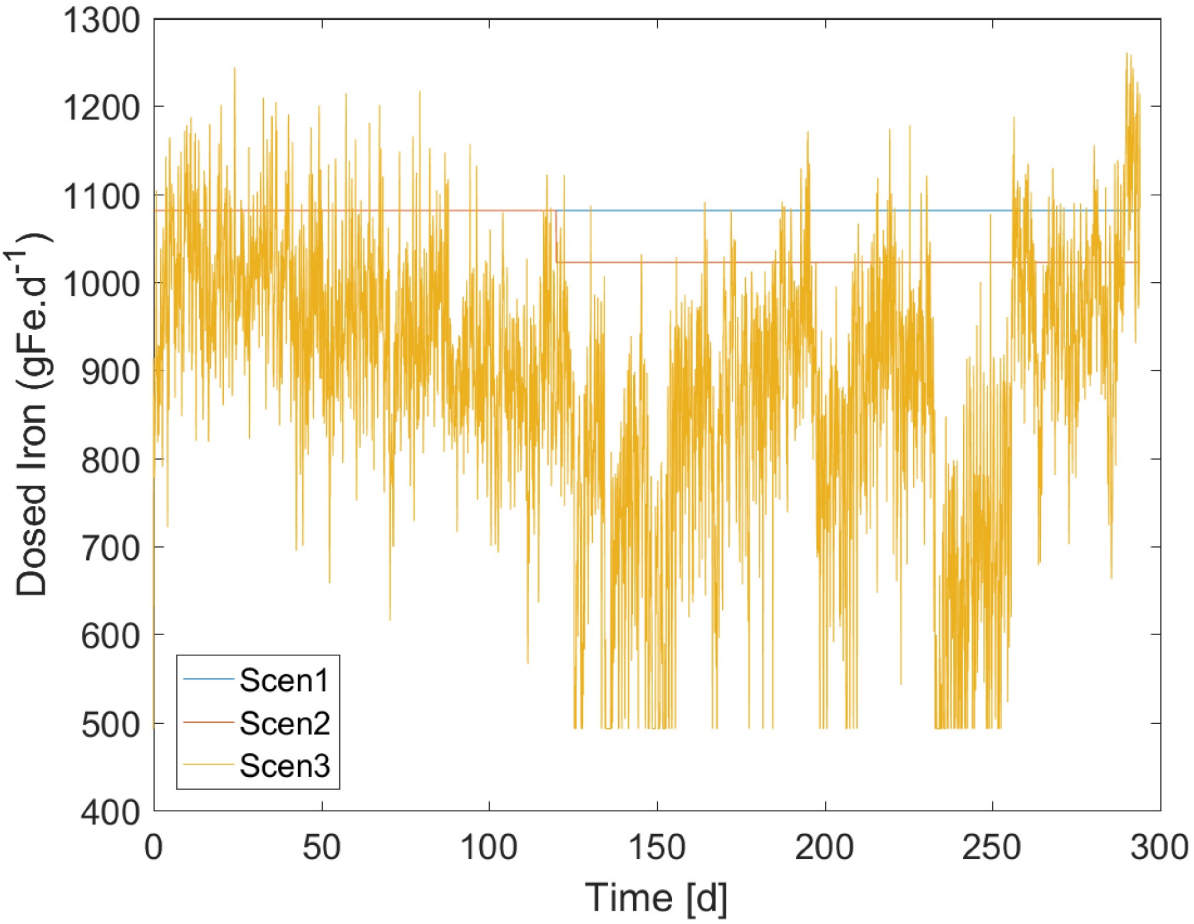

Figure 8 *– Total amount of added iron ($FeSO_4$ and $FeCl_3$) at the three dosing locations for Scenarios 1 - 3.*

Figure 9 shows the results of concentration profiles of ammonia nitrogen in the secondary effluent for the first three scenarios. The simulation results indicate that the concentrations of ammonia nitrogen in the effluent decrease by approximately 8.7% for the 2nd scenario and decrease by 8.2% for the 3rd scenario, respectively. The spikes in the simulated ammonia concentrations correspond very well to lower concentrations of soluble phosphate in the bioreactors. The overall results indicated that phosphorus deficiency due to simultaneous precipitation may be detrimental to autotrophic nitrifying bacteria which require enough phosphorus for cell growth. It should be noted that phosphorus limitation can occur when the concentration of phosphorus is in the range of 0.1 to 0.3 $gP.m^{-3}$ (Metcalf & Eddy, 2004). However, the adverse effects caused by lower P concentrations were avoided in the model by increasing the value of the autotrophic saturation coefficient for phosphate (K_p) from 0.01 to 0.001 $gP.m^{-3}$. This could explain the necessity to control the level of bioreactor phosphate

concentrations to reduce the extent to which biological processes may be inhibited under conditions of low bioreactor phosphate concentrations.

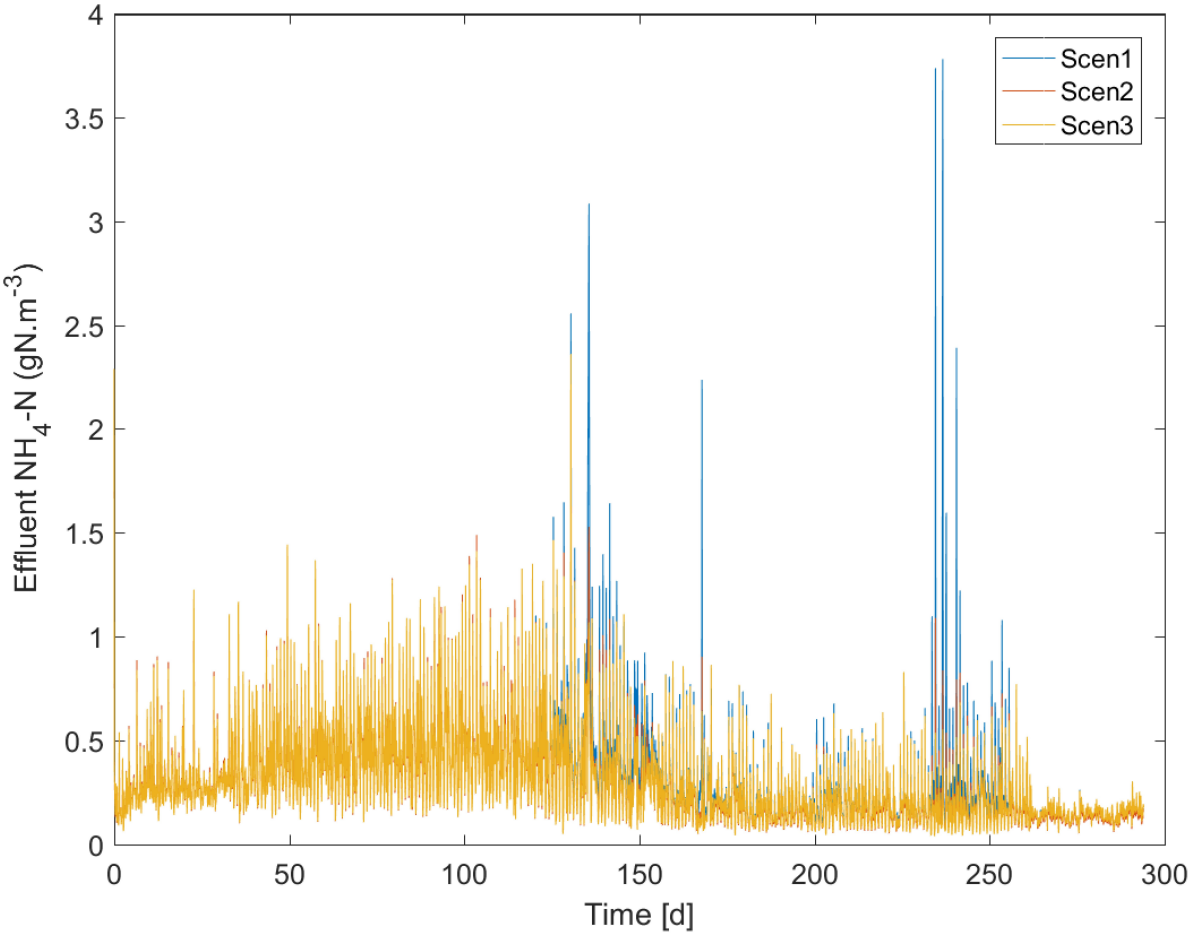

Figure 9 *– Dynamic simulations of ammonia nitrogen in the treatment plant outflow for Scenarios 1 - 3.*

3.4.2 Impact of controlling iron salt ($FeSO_4$ & $FeCl_3$) dosing

The impact of imposing a basic control and operational strategy for maintaining the concentration of phosphate below the required future standard was carried out for demonstration purposes. As shown in Scenario 1, when the pilot plant model was simulated under dynamic conditions with constant feed of $FeSO_4$ (aerobic tank) and $FeCl_3$ (MBR tanks), the effluent phosphorus concentration varied considerably due to fluctuations in the flow and load. Based on open-loop simulation results, the pilot plant could not consistently meet the effluent standards. In other words, if PO_4 in the effluent is not controlled, its content will easily drift out of the acceptable performance range. Furthermore, in some instances, when the concentrations of P were low in the influent, this led to very low concentrations

(below 0.15 $gP.m^{-3}$) in the effluent, which indicated that dosing could be unnecessary under such conditions. Consequently, a simultaneous precipitation control scheme was deemed necessary and was implemented to maintain the PO_4 concentration in the effluent at 0.15 $gP.m^{-3}$ using a PI controller to adjust the dosage of $FeCl_3$ to the membranes. In addition, $FeSO_4$ addition to the second aerobic tank was controlled towards a set point of 0.2 $gP.m^{-3}$ in the effluent. The PO_4 sensor and actuator were modelled without noise or delay, their performances were assumed to be ideal.

The results in Figure 7 (Scenario 3) indicate that the implemented PO_4 strategy enabled the plant to reach P effluent concentrations of about 0.15 $gP.m^{-3}$ as stipulated by the future effluent quality standard, while at the same time making sure that the coagulants were only added when required. However, it should be pointed out that higher amounts of Fe salts were required with PO_4 controllers. For example, when the sensor for $FeSO_4$ dosage was at the same location (effluent) as the one for $FeCl_3$ dosage, the simulation indicates that only the $FeCl_3$ controller with the lowest set point (0.15$gP.m^{-3}$) was working. Moving the location of the $FeSO_4$ controller before the pre-anoxic tank led to a reduction of iron coagulant by 15% since both controllers were working as per set criteria. Controlling Fe salts dosing also provides additional benefits of maintaining optimal conditions for nitrification/denitrification processes. Previous studies have shown that biological nutrient removal mechanisms function less well in the presence of chemical precipitation under conditions where the P concentration in the activated sludge is low and potentially limiting (Philips *et al.*, 2015). In other words, the chemical precipitation mechanism limits the extent to which biological nutrient removal potential can be utilised by removing other nutrients in the system. This could be an indication of limiting P conditions where denitrifying microorganisms have been depressed or deprived of essential growth nutrients. Such conditions with low P may be prevalent in WWTPs with MBRs and chemical P removal, such as the pilot-scale plant under study, designed to reach very low effluent P content. Therefore, it is recommended to control the addition of iron salts. When the P controllers are maintained at their set points by closed-loop control, the WWTP will achieve lower P values in the effluent.

3.4.3 Impact of iron dosing location

To maximize the removal of phosphorus in the presence of iron salts, different iron dosing locations including the aerobic tank, anoxic tank and RAS/DEOX stream were investigated. Given that the dissolved oxygen content of the RAS/DEOX stream from the MBRs is high

and can have impact on the denitrification process in the anoxic tank, simulations were used to analyse whether adding Fe(II) salts in this location could provide additional benefits in reducing the oxygen level being recirculated to the activated sludge. Figure 10 shows the results of the simulated effluent P concentrations from the impact of $FeSO_4$ dosing at the three different locations in the activated sludge system for Scenarios 1 (blue solid line), 4 (red solid line) and 5 (yellow solid line). The dosing location in each case was changed at the beginning of the simulation (from time $t = 0$).

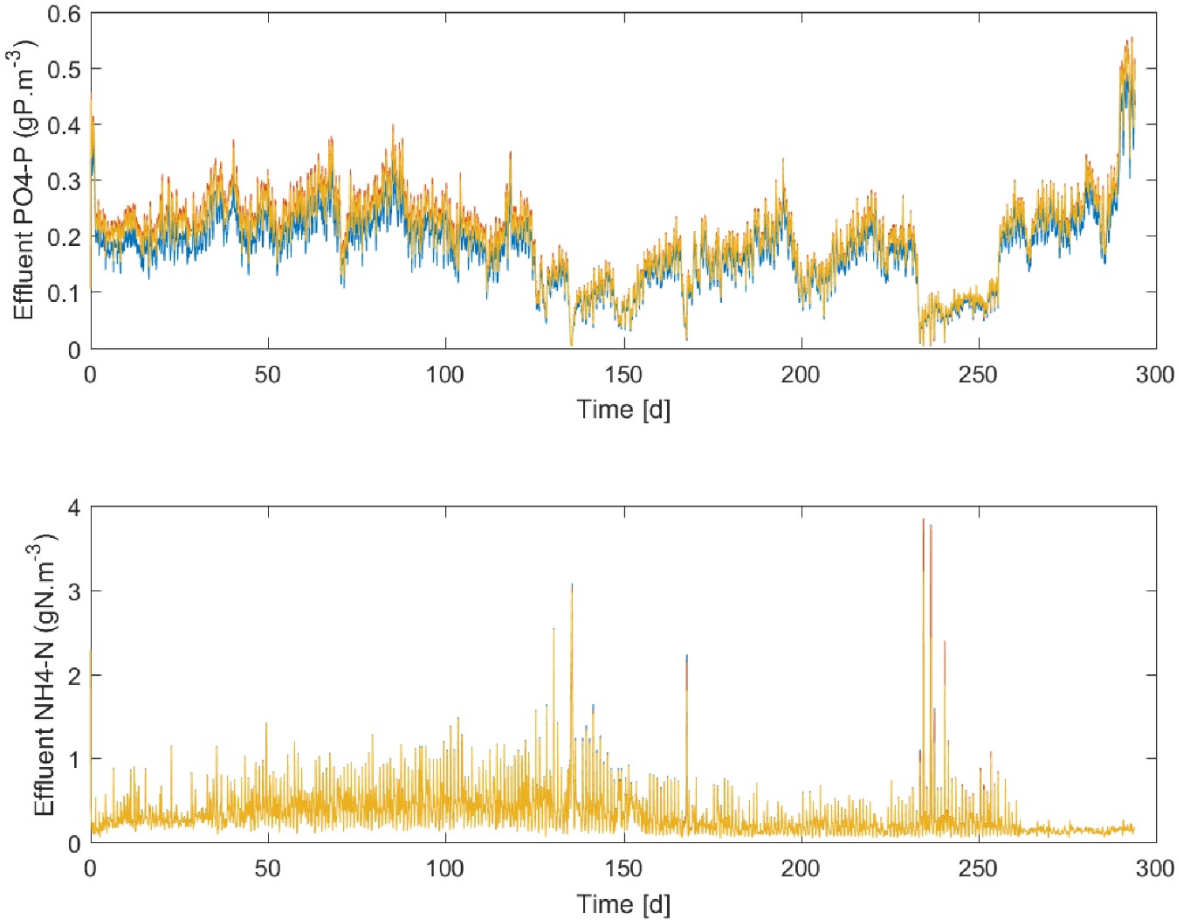

Figure 10 *– Dynamic simulations of the soluble phosphate and ammonia nitrogen in the treatment plant outflow for Scenarios 4, 5 and 6. The blue solid, red solid and yellow solid lines show the simulation results for the Scenario 4, Scenario 5 and the Scenario 6, respectively.*

In comparison to Scenario 1 (default location), the simulation results indicate that the concentrations of phosphorus in the effluent increase by roughly 17% and 13% for the 4th and 5th scenarios, respectively. Whereas in the case of ammonia nitrogen concentration in the

effluent, the reduction is small: 0.96% in the 4th scenario and 1.8% in the 5th scenario. The decrease of nitrate in the effluent in the fifth scenario is due to the decreased contribution of RAS/DEOX oxygen entering the anoxic tank. In general, the results show that iron addition at these locations have a very slight impact on phosphorus removal performance. The implication would be that $FeSO_4$ dosing should be fed at an aeration stage in the activated sludge process, where there is good mixing. When dosed prior to the aeration tank, ferrous salts will dissolve and then some of the resulting Fe^{2+} will be oxidized to ferric iron by nitrate (anoxic zone), whereas the remaining will undergo oxidation in the aerobic zone.

3.5 Model performance and limitations

The overall results of this study demonstrate the usefulness of a plant-wide model incorporating iron transformation and precipitation. Such a model provides mechanistic analysis of phosphorous transport and partitioning and could be used to develop control strategies to optimize simultaneous precipitation while maximizing the nutrient removal. However, it should be pointed out that the application of an activated sludge model combined with chemical P removal requires fully characterised and adequately fractionated COD components and additional influent characterization of soluble chemical components, particularly iron species, to incorporate in the physico-chemical module. The pilot plant under study only carries out limited routine measurements, which also include very limited measurements of soluble chemical components. To increase the accuracy of predicting simultaneous precipitation, it would be essential to perform additional measurements to cover all the relevant components, including iron speciation, that play a significant role in modelling simultaneous precipitation. The timing of the project did not allow a systematic measurement campaign to be carried out due to summer holidays. However, if the proposed plant-wide model is to be used for process performance and optimization for chemical dosing, adequate influent characterization will be required.

While the concentrations of Fe(II) and Fe(III) were not measured as part of routine measurements, underlying assumptions of chemical P removal in the model shed light through the simulations. When iron sulphate was added to the aerobic tank, the majority of ferrous iron was oxidized and converted to insoluble HFO due to abundance of dissolved oxygen (DO > 2.0 $g.m^{-3}$). Removal of P through direct precipitation of vivianite ($Fe_3(PO_4)_2 \cdot 8H_2O$) appears very unlikely at the minimum Fe(II) concentration since the driving force for forming this ferrous phosphate mineral is very low. Furthermore, higher DO

levels (above 4 $g.m^{-3}$) in the return activated sludge due higher aeration in the membrane tanks would likely hamper the formation of any ferrous phosphate in MBRs. In prevailing aerobic conditions, the precipitation of vivianite appears to be very slow and likely restricted to anaerobic pockets (Wu *et al.*, 2015). As a result, the addition of Fe(II) salts to either an anoxic or aerobic zone should facilitate the formation of HFO precipitates and $FePO_4$, and remove phosphates in the mixed liquor. However, this assumption is in contrast to other studies, which have hypothesized vivianite as a possible route for phosphorus removal in activated sludge (Frossard *et al.*, 1997; Wilfert *et al.*, 2016). In this respect, to describe reliably the movements and cycling of iron precipitates, iron-phosphorus speciation tests should be carried out in the sludge for the pilot-plant under study with prevailing oxidizing conditions, which have likely favoured the formation of Fe(III)–phosphorus minerals.

The model analysis focused quite extensively on the fate of iron and phosphorus in the activated sludge system. However, it should be pointed out that the plant-wide model used included a sludge treatment train which consisted of sludge thickening, digestion and dewatering. During anaerobic digestion of waste activated sludge, the iron is released as a result of iron phosphate dissolution leading to its increased soluble concentration of iron. Sludge digestion also releases sulphide due to sulphate reduction and the degradation of sulphur-containing organics (Batstone *et al.*, 2002). The released sulphide will preferentially bind with iron to form iron sulphide minerals leading to low concentration of dissolved sulphide and hence reduced H_2S concentration in the gas phase (Ge *et al.*, 2013).

4 Conclusions

The present study has demonstrated that an integrated model (ASM2d, ADM1, physico-chemical model) is suitable to model biological nutrient and chemical P removal precipitation. In the physico-chemical framework, fast reactions in the aqueous phase were modelled using equilibrium thermodynamics, while time-dependent reactions (such as precipitation) were modelled using dedicated kinetic rate laws. The integrated model had the least level of complexity but gave reasonable results with pilot-scale data. The following were key modelling outcomes:

1) Despite limited operational and routine pilot-scale data, the plant-wide model was able to replicate with acceptable accuracy the trends in effluent soluble ammonia and phosphate, suspended solids and other variables under steady state and dynamic conditions. Simultaneous precipitation was the main mechanism that removed phosphorus during wastewater treatment.
2) The amount and types of existing iron mineral phases present in the mixed liquor was one of the most influential factors for precipitation reactions. In a system without bio-P process, phosphorus removal is a result of P adsorption and co-precipitation through the accumulated HFO, as well as a competing reaction of iron phosphate. Ferric iron precipitates originated from ferrous iron oxidation in wastewater affect the removal of P in the activated sludge system and impact the cycling of P in wastewater treatment within a plant-wide framework.
3) The simulations confirmed that the modelling approach was valid, particularly the dependency on pH, which showed a strong effect. The ratio of Fe/P was also identified as an influential factor that (where possible) should be set based on the effluent P target. At higher ratios, lower P concentrations are expected in the influent. However, when the P concentration in the mixed liquor is very low, increasing the ratio does not translate linearly in further removal of P.
4) The dosing point of $FeSO_4$ in the activated sludge system was analysed for three different locations: aerobic, anoxic and RAS/DEOX tanks. Feeding at the aerobic tank had a slightly higher effect on the chemical P removal; consequently, this location is preferable due to high DO and good mixing conditions that could maximize the formation of HFO particulates and iron phosphate.

5 Recommendations: operational and control strategies

The modelling results in this study suggest that current pilot-plant work has shown that effective nutrient removal can be achieved in a conventional activated system with membrane bioreactors and chemical P removal. The model was able to predict nitrification, as indicated by the effluent total and ammonia nitrogen concentrations consistently below 6 and 2 $gN.m^{-3}$, respectively. On other hand, chemical phosphorus removal reduced effluent total phosphorus values to well below 0.15 mg/L. Modelling experience of the pilot-plant in this study suggest the following recommendations to achieve effective P removal:

1) Chemical precipitation takes place through fresh iron precipitates, which are amorphous, metastable and their transformation into more stable phases during aging results in P removal. The pH, Fe/P molar ratio and sludge age in the wastewater treatment affect the aging of the iron-precipitates; these factors should be monitored for effective P removal.
2) The most appropriate dosing point of $FeSO_4$ is in an aerated zone where the Fe(II) oxidation is more efficient.
3) Since iron salts are added in the pilot-system, controlling $FeSO_4$ and $FeCl_3$ is essential for optimal P removal while at the same time avoiding overdosing during periods when influent P is very low or when the effluent quality is below 0.15 $gP.m^{-3}$. This aspect is also important for suitable biological processes, such as nitrification, which require P for microbial metabolism.
4) Sensors for controlling $FeSO_4$ addition should be placed before the point where $FeCl_3$ is dosed, whereas the sensor for the latter should be located at the effluent.
5) Prior knowledge was used to identify phosphorus-containing precipitates that would form under the operating conditions of the pilot-plant. Given that influent characteristics may affect the formation or inhibition of some of these minerals, experimentally-based techniques, e.g. X-ray diffraction (XRD) and Mössbauer spectroscopy as used in Wilfert *et al.* (2016), may be required in order to provide improved characterization of the iron-precipitates in the activated sludge.

References

APHA (2012). Standard methods for the examination of water and wastewater, American Public Health Association, Washington, USA.

Andersson, S., Ek, P., Berg, M., Grundestam, J., & Lindblom, E. (2016). Extension of two large wastewater treatment plants in Stockholm using membrane technology. *Water Practice and Technology*, *11*(4), 744-753.

Bligh, M.W., Maheshwari, P., & David Waite, T. (2017). Formation, reactivity and aging of amorphous ferric oxides in the presence of model and membrane bioreactor derived organics, *Water Research, 124*, 341-352.

Henze, M., Harremoes, P., la Cour Jansen, J., & Arvin, E. (2002). Wastewater Treatment: Biological and Chemical Processes. Springer, Berlin, Germany.

Batstone, D.J., Keller, J., Kalyuzhnyi, S.V., Pavlostathis, S.G., Rozzi, A., Sanders, W.T.M., Siegrist, H., & Vavilin, V.A. (2002). Anaerobic Digestion Model No. 1, IWA Publishing, London, UK.

Daigger, G.T., Crawford, G.V., & Johnson, B.R. (2010). Full-scale assessment of the nutrient removal capabilities of membrane bioreactors. *Water Environment Research*, *82*(9), 806-818.

De Haas, D.W., Wentzel, M.C., & Ekama, G.A. (2001). The use of simultaneous chemical precipitation in modified activated sludge systems exhibiting biological excess phosphate removal: Part 5: Experimental periods using a ferrous-ferric chloride blend. *Water SA*, *27*(2), 117-134.

De Haas, D.W., Ekama, G.A., & Wentzel, M.C. (2000a). The use of simultaneous chemical precipitation in modified activated sludge systems exhibiting biological excess phosphate removal – Part 1: Literature review. *Water SA, 26*(4), 439-452.

De Haas, D.W., Ekama, G.A., & Wentzel, M.C. (2000b). The use of simultaneous chemical precipitation in modified activated sludge systems exhibiting biological excess phosphate removal – Part 4: Experimental periods using ferric chloride. *Water SA*, *26*(4), 485-504.

Ekama, G.A. (2010). The role and control of sludge age in biological nutrient removal activated sludge systems. *Water Science and Technology*, *61*(7), 1645-1652.

EPA (Environmental Protection Agency) (2010). Nutrient Control Design Manual, State of Technology. The Cadmus Group Inc., USA.

Flores-Alsina, X., Kazadi Mbamba, C., Solon, K., Vrecko, D., Tait, S., Batstone, D.J., Jeppsson, U., & Gernaey, K.V. (2015). A plant-wide aqueous phase chemistry module describing pH variations and ion speciation/pairing in wastewater treatment process models. *Water Research*, *85*, 255-265.

Flores-Alsina, X., Solon, K., Kazadi Mbamba, C., Tait, S., Gernaey, K.V., Jeppsson, U., & Batstone, D.J. (2016). Modelling phosphorus (P), sulfur (S) and iron (Fe) interactions during dynamic simulations of anaerobic digestion processes. *Water Research, 95*, 370-382.

Frossard, E., Bauer, J.P., & Lothe, F. (1997). Evidence of vivianite in $FeSO_4$-flocculated sludges. *Water Research, 31*(10), 2449-2454.

Ge, H., Zhang, L., Batstone, D., Keller, J., & Yuan, Z. (2013). Impact of iron salt dosage to sewers on downstream anaerobic sludge digesters: Sulfide control and methane production. *Journal of Environmental Engineering, 139*(4), 594-601.

Gernaey, K.V., Flores-Alsina, X., Rosen, C., Benedetti, L., & Jeppsson, U. (2011). Dynamic influent pollutant disturbance scenario generation using a phenomenological modelling approach. *Environmental Modelling & Software, 26*(11), 1255-1267.

Gernaey, K.V., Jeppsson, U., Vanrolleghem, P.A., & Copp, J.B. (2014). Benchmarking of control strategies for wastewater treatment plants, IWA Publishing, London, UK.

Grady Jr, C.L., Daigger, G.T., Love, N.G., & Filipe, C.D. (2011). Biological wastewater treatment, CRC Press, Boca Raton, USA.

Gustafsson, J.P. (2015). Visual MINTEQ version 3.1, beta, Available at http://vminteq.lwr.kth.se/download/.

Hauduc, H., Takács, I., Smith, S., Szabo, A., Murthy, S., Daigger, G.T., & Spérandio, M. (2015). A dynamic physicochemical model for chemical phosphorus removal. *Water Research, 73*, 157-170.

Henze, M., Gujer, W., Mino, T., & van Loosdrecht, M.C.M. (2000). Activated sludge models ASM1, ASM2, ASM2d and ASM3. IWA Publishing, London, UK.

Henze, M., Gujer, W., Mino, T., Matsuo, T., Wentzel, M., & Marais, G.v.R. (1995). Wastewater and biomass characterization for the Activated Sludge Model No. 2: Biological phosphorus removal. *Water Science and Technology, 31*(2), 13-23.

Henze, M., Harremoes, P., Cour Jansen, J. la, & Arvin, E. (2002). Wastewater Treatment: Biological and Chemical Processes. Springer, Berlin, Germany.

Jeppsson, U., Pons, M.N., Nopens, I., Alex, J., Copp, J.B., Gernaey, K.V., Rosen, C., Steyer, J.P., & Vanrolleghem, P.A. (2007). Benchmark Simulation Model No 2: General protocol and exploratory case studies. *Water Science and Technology*, *56*(8), 67-78.

Jiang, T., Myngheer, S., De Pauw, D.J.W., Spanjers, H., Nopens, I., Kennedy, M.D., Amy, G. & Vanrolleghem P.A. (2008). Modelling the production and degradation of soluble microbial products (SMP) in membrane bioreactors (MBR). *Water Research, 42*, 4955–4964.

Judd, S. (2008). The status of membrane bioreactor technology. *Trends in Biotechnology*, *26*(2), 109-116.

Kazadi Mbamba, C., Batstone, D.J., Flores-Alsina, X., & Tait, S. (2015a). A generalised chemical precipitation modelling approach in wastewater treatment applied to calcite. *Water Research, 68*, 342-353.

Kazadi Mbamba, C., Tait, S., Flores-Alsina, X., & Batstone, D.J. (2015b). A systematic study of multiple minerals precipitation modelling in wastewater treatment. *Water Research, 85*, 359-370.

Kazadi Mbamba, K., Flores-Alsina, X., Batstone, D.J., & Tait, S. (2016). Validation of a plant-wide phosphorus modelling approach with minerals precipitation in a full-scale WWTP. *Water Research*, *100*, 169-183.

Mamais, D., Jenkins, D., & Pitt, P. (1993). A rapid physical-chemical method for the determination of readily biodegradable soluble COD in municipal wastewater. *Water Research*, *27*(1), 195-197.

Metcalf & Eddy (2004). Wastewater Engineering: Treatment and Reuse (Tchobanoglous, G., Burton, F. and Stensel, H. D., Eds., 4th ed.). Boston: McGraw-Hill, USA.

Otterpohl, R., & Freund, M. (1992). Dynamic models for clarifiers of activated sludge plants with dry and wet weather flows. *Water Science and Technology, 26*(5-6), 1391-1400.

Philips, S., Rabaey, K., & Verstraete, W. (2003). Impact of iron salts on activated sludge and interaction with nitrite or nitrate. *Bioresource Technology*, *88*(3), 229-239.

Siegrist, H., & Tschui, M. (1992). Interpretation of experimental data with regard to the activated sludge model no. 1 and calibration of the model for municipal wastewater treatment plants. *Water Science and Technology, 25*(6), 167-183.

Solon, K., Flores-Alsina, X., Mbamba, C.K., Ikumi, D., Volcke, E.I.P., Vaneeckhaute, C., Ekama, G., Vanrolleghem, P.A., Batstone, D.J., Gernaey, K.V., & Jeppsson, U. (2017). Plant-wide modelling of phosphorus transformations in wastewater treatment systems: Impacts of control and operational strategies. *Water Research*, *113*, 97-110.

Wang, Y., Tng, K.H., Wu, H., Leslie, G., & Waite, T.D. (2014). Removal of phosphorus from wastewaters using ferrous salts – A pilot scale membrane bioreactor study. *Water Research*, *57*, 140-150.

Wilfert, P., Mandalidis, A., Dugulan, A.I., Goubitz, K., Korving, L., Temmink, H, Witkamp, G.J., & van Loosdrecht, M.C.M. (2016). Vivianite as an important iron phosphate precipitate in sewage treatment plants. *Water Research, 104*, 449-460.

Wu, H., Ikeda-Ohno, A., Wang, Y., & Waite, T.D. (2015). Iron and phosphorus speciation in Fe-conditioned membrane bioreactor activated sludge. *Water Research*, *76*, 213-226.

Appendix

Table A.1 *– Analysis results for grab and daily composite samples from the pilot-plant (12/07/2017 to 19/07/2017).*

Date	Sampling Type	Sampling Point	COD-Cr (605 nm) ($gCOD.m^{-3}$)	COD-Cr (448 nm) ($gCOD.m^{-3}$)	COD-Cr (448 nm) filtered ($gCOD.m^{-3}$)	TOC ($gC.m^{-3}$)	TIC ($gC.m^{-3}$)	DOC ($gC.m^{-3}$)	TSS ($gSS.m^{-3}$)
2017-07-12	Grab	Influent		180	49	50		18.4	
2017-07-12	Grab	Primary effluent		190	100	66		39.4	
2017-07-12	Daily composite	Influent					38		210
2017-07-12	Daily composite	Primary effluent					60		120
2017-07-12	Daily composite	Permeate					32		0
2017-07-13	Grab	Influent	550		100	120		35.1	
2017-07-13	Grab	Primary effluent	180		71	48		24.5	
2017-07-13	Daily composite	Influent					43		200
2017-07-13	Daily composite	Primary effluent					50		120
2017-07-13	Daily composite	Permeate					23		0
2017-07-14	Grab	Influent	440		120	91		40.1	
2017-07-14	Grab	Primary effluent		120	40	38		15.5	
2017-07-14	Daily composite	Influent					66		220
2017-07-14	Daily composite	Primary effluent					67		140
2017-07-14	Daily composite	Permeate					17		0
2017-07-19	Grab	WAS							6800

Table A.2 *– Analysis results for grab and daily composite samples from the pilot-plant (12/07/2017 to 19/07/2017).*

Date	Type of sampling	Sampling Point	GR (VSS) ($g.m^{-3}$)	VSS (% of SS)	pH	T (during pH-analysis) (oC)	TP ($gP.m^{-3}$)	Cl- ($g.m^{-3}$)	Sulphate ($gS.m^{-3}$)
2017-07-12	Grab	Influent							
2017-07-12	Grab	Primary effluent							
2017-07-12	Daily composite	Influent	120	0.571429	7.4	20.9	5	74	48
2017-07-12	Daily composite	Primary effluent	100	0.833333	7.5	20.8	4.8	74	50
2017-07-12	Daily composite	Permeate	0		7.9	20.4		73	
2017-07-13	Grab	Influent							
2017-07-13	Grab	Primary effluent							
2017-07-13	Daily composite	Influent	170	0.85	7.4	20.8	5.9	77	49
2017-07-13	Daily composite	Primary effluent	100	0.833333	7.5	20.5	5.3	77	56
2017-07-13	Daily composite	Permeate	0		7.9	20.4	0.81	76	
2017-07-14	Grab	Influent							
2017-07-14	Grab	Primary effluent							
2017-07-14	Daily composite	Influent	200	0.909091	7.1	20.1	6.4	77	46
2017-07-14	Daily composite	Primary effluent	110	0.785714	7.2	20.1	5	76	62
2017-07-14	Daily composite	Permeate	0		7.9	20.9	0.29	77	
2017-07-19	Grab	WAS	4100	0.602941			250		

Table A.3 *– Analysis results for grab and daily composite samples from the pilot-plant (12/07/2017 to 19/07/2017).*

Date	Type	Point	Na ($g.m^{-3}$)	K ($g.m^{-3}$)	Ca ($g.m^{-3}$)	Fe ($g.m^{-3}$)	Mg ($g.m^{-3}$)	Al ($g.m^{-3}$)	acetic acid ($g.m^{-3}$)
2017-07-12	Grab	Influent							13
2017-07-12	Grab	Primary effluent							23
2017-07-12	Daily composite	Influent	63	21	40	0.98	7.1	0.76	
2017-07-12	Daily composite	Primary effluent	63	21	39	0.68	6.9	0.48	
2017-07-12	Daily composite	Permeate		18		0.087			
2017-07-13	Grab	Influent							23
2017-07-13	Grab	Primary effluent							18
2017-07-13	Daily composite	Influent	64	21	42	1.2	7.4	0.7	
2017-07-13	Daily composite	Primary effluent	63	20	40	6.9	7.3	0.43	
2017-07-13	Daily composite	Permeate		19		0.098			
2017-07-14	Grab	Influent							25
2017-07-14	Grab	Primary effluent							21
2017-07-14	Daily composite	Influent	66	22	40	1.6	7.5	0.76	
2017-07-14	Daily composite	Primary effluent	62	21	37	10	7.6	0.36	
2017-07-14	Daily composite	Permeate		20		0.1			
2017-07-19	Grab	WAS				1100			